NASA/CR—2002-211562

SSP Technology Investigation of a High-Voltage DC-DC Converter

J.A. Pappas and W.M. Grady
University of Texas at Austin, Austin, Texas

June 2002

The NASA STI Program Office . . . in Profile

Since its founding, NASA has been dedicated to the advancement of aeronautics and space science. The NASA Scientific and Technical Information (STI) Program Office plays a key part in helping NASA maintain this important role.

The NASA STI Program Office is operated by Langley Research Center, the Lead Center for NASA's scientific and technical information. The NASA STI Program Office provides access to the NASA STI Database, the largest collection of aeronautical and space science STI in the world. The Program Office is also NASA's institutional mechanism for disseminating the results of its research and development activities. These results are published by NASA in the NASA STI Report Series, which includes the following report types:

- TECHNICAL PUBLICATION. Reports of completed research or a major significant phase of research that present the results of NASA programs and include extensive data or theoretical analysis. Includes compilations of significant scientific and technical data and information deemed to be of continuing reference value. NASA's counterpart of peer-reviewed formal professional papers but has less stringent limitations on manuscript length and extent of graphic presentations.

- TECHNICAL MEMORANDUM. Scientific and technical findings that are preliminary or of specialized interest, e.g., quick release reports, working papers, and bibliographies that contain minimal annotation. Does not contain extensive analysis.

- CONTRACTOR REPORT. Scientific and technical findings by NASA-sponsored contractors and grantees.

- CONFERENCE PUBLICATION. Collected papers from scientific and technical conferences, symposia, seminars, or other meetings sponsored or cosponsored by NASA.

- SPECIAL PUBLICATION. Scientific, technical, or historical information from NASA programs, projects, and missions, often concerned with subjects having substantial public interest.

- TECHNICAL TRANSLATION. English-language translations of foreign scientific and technical material pertinent to NASA's mission.

Specialized services that complement the STI Program Office's diverse offerings include creating custom thesauri, building customized data bases, organizing and publishing research results . . . even providing videos.

For more information about the NASA STI Program Office, see the following:

- Access the NASA STI Program Home Page at ***http://www.sti.nasa.gov***

- E-mail your question via the Internet to help@sti.nasa.gov

- Fax your question to the NASA Access Help Desk at 301–621–0134

- Telephone the NASA Access Help Desk at 301–621–0390

- Write to:
  NASA Access Help Desk
  NASA Center for AeroSpace Information
  7121 Standard Drive
  Hanover, MD 21076

NASA/CR—2002-211562

SSP Technology Investigation of a High-Voltage DC-DC Converter

J.A. Pappas and W.M. Grady
University of Texas at Austin, Austin, Texas

Prepared under Contract NAS3–00135

National Aeronautics and
Space Administration

Glenn Research Center

June 2002

Available from

NASA Center for Aerospace Information
7121 Standard Drive
Hanover, MD 21076

National Technical Information Service
5285 Port Royal Road
Springfield, VA 22100

Available electronically at http://gltrs.grc.nasa.gov/GLTRS

TABLE OF CONTENTS

1 Introduction 1

1.1 Extension of previous RATVS and converter development 3

2 DC-DC converter circuits for space applications 3

2.1 NASA requirements 3

2.2. Overview of the Jones chopper circuit 4

2.2.1 Design of the chopper portion of the circuit 4

2.2.2 Design of the load portion of the circuit 6

2.3 Preliminary examples with low voltage 7

2.3.1 Example #1 – Input = 1,000 V, 25 A (chopped), output = 400 V, 25 A, 10 kW; frequency = 1kHz 7

2.3.2 Scaling formulas 8

2.3.3 Example #2 – Modification of example #1 to boost the load voltage 9

2.3.4 Example #3 – Scaling of example #1 for input = 15kV, 10kA (chopped); output = 12 kV, 10 kA, 120 MW; frequency = 1 kHz 9

2.3.5 Example 4 – Reconfiguration of Jones chopper to construct a boost converter with low ripple source current: input = 1,000 V, 10 A (low ripple); output = 1,667 V, 6 A, 10 kW; frequency = 1 kHz 10

2.4 High voltage examples with modular one-twelfth power and with full power converter 11

2.4.1 One-twelfth modular power converter suitable for paralleling 11

2.4.2 Full power circuit 13

2.5 Proposed proof-of-concept prototype 13

3 Triggered vacuum switches 13

4 Component design for a modular DC-DC converter 16

4.1 Design of triggered vacuum switches for long life 17

4.2 Design of the filter inductor and of the autotransformer 23

5 Potential technological developments 23

5.1 The rod array triggered vacuum switch 23

5.2 The filter inductor and the autotransformer 24

6 Summary and Recommendations 25

REFERENCES 26

LIST OF TABLES

1 Electrode candidate materials in order of initil preference 27
2 Electrode candidate materials in order of k_m 27
3 Electrode candidate materials in order of conductivity 27
4 Preliminary design specifications 27

LIST OF FIGURES

1 Commercially-available RATVS 28

2 Jones chopper for Example #1 with logic clocks operating at 1 kHz and duty cycle 0.40 *(Note: the coefficient of coupling k in the coupled coils is negative to reverse the dot polarity of one of the windings)* 28

3 Load voltage for 10 kW Jones chopper in figure 2.1 29

4 Jones chopper modified with booster transformer 29

5 Load voltage for 10 kW Jones chopper in figure 2.3 30

6 100 MW Jones chopper 30

7 Load voltage for 100 MW Jones chopper of figure 2.5 31

8 10 kW Jones chopper, modified to operate as a boost converter 31

9 Load voltage for 10 kW Jones chopper-booster of figure 2.7 32

10 Source current for 10 kW Jones chopper-booster of figure 2.7 32

11 One-twelfth modular power converter suitable for paralleling (output 40 kV, 2,083 A, 83.3 MW) 33

12 Load voltage for one-twelfth power converter (entire simulation) 33

13 Load voltage for one-twelfth power converter (zoom-in of steady-state region) 34

14 Filter inductor current (zoom-in of steady-state region) 34

15 RATVS#1 firing pulse, and commutating capacitor C current (zoom-In of steady-state region) 35

16 RATVS#1 firing pulse and coupled coil currents (left to right) (zoom-in of steady-state region) 35

17 RATVS#1 firing pulse and commutating capacitor C voltage (zoom-in of steady-state region) 36

18 Full power converter (output 40 kV, 25 kA, 1,000 MW) 36

19 Proposed proof of concept prototype 37

20 Load voltage for proof of concept prototype (entire simulation) 37

21 Load voltage for proof of concept prototype (zoom-in of steady-state region) 38

22 Filter inductor current (zoom-in of steady-state region) 38

23 RATVS#1 firing pulse, and commutating capacitor C current (zoom-in of steady-state region) 39

24 RATVS#1 firing pulse and coupled coil currents (left to right) (zoom-in of steady-state region) 39

25 RATVS#1 firing pulse and commutating capacitor C voltage (zoom-in of steady-state region) 40

26 Open view of a rod array triggered vacuum switch 40

27 The cathode half of a six electrode RATVS (from [1]) 41

28 Conceptual design of the rod of an electrode with forced convection cooling 42

29 Filter inductor 43

30 Autotransformer 44

1 Introduction

The goal of this project was to establish the feasibility of a high-voltage DC-DC converter based on a rod-array triggered vacuum switch (RATVS) for the Space Solar Power system. The RATVS has many advantages over silicon and silicon-carbide devices. The RATVS is attractive for this application because it is a high-voltage device that has already been demonstrated at current in excess of the requirement for an SSP device and at much higher per-device voltage than existing or near-term solid state switching devices. The RATVS packs a much higher specific power rating than any solid-state device and it is likely to be more tolerant of its surroundings in space. In addition, pursuit of an RATVS-based system would provide NASA with a nearer-term and less expensive power converter option for the SSP.

RATVS characteristics and advantages include:

- its electrodes exhibit very little wear and the switch has a low voltage drop
- it can operate much like a thyristor
- it is a fault tolerant device
- it can operate at high voltage. RATVS have already been demonstrated at 84 kV
- realization of a 100 kV, 10-20 kA RATVS is well within the reach of near-term technology.

The objectives of the project were to:

- develop the electrical requirements for an RATVS capable of operating at 100 kV and recover in the forward and reverse directions after passing up to 15 kA at the required switching frequency and rates of current rise and fall
- develop an electrical system performance model of a DC-DC converter that can operate at 100 kV and 1 GW using the Saber® simulation environment
- develop an preliminary concept electrical design for an RATVS-based DC-DC converter that can operate at 100 kV and 1 GW.

A section view of a commercially available version of the device is shown in figure 1. It is a high-power vacuum switch that was specifically designed to operate in the diffuse arc mode. The electrodes are arranged so that the self-magnetic field forces the discharge arc to remain diffuse rather than to concentrate into constricted channels; therefore no anode spots are formed. As a result, the RATVS electrodes exhibit very little wear and the switch has a low voltage drop. In addition, the RATVS can operate much like a thyristor. It can be triggered to initiate forward conduction and it will clear and recover following a current zero [1,2].

RATVSs are fault tolerant devices. That is, faults such as over-current or current reversal are unlikely to cause an RATVS to fail. Current reversal has been repeatedly demonstrated on a 25 kV device [2]. In addition, RATVSs are likely to be less affected by background radiation and they can operate over an extremely wide temperature range.

One of the primary advantages of the RATVS is its high per-device operating voltage. Off-the-shelf devices that operate at 20 kV are readily available. The results for experimental tubes are very encouraging. In experimental devices, withstand voltages of 460 kV (impulse) and 240 kV (hi-pot) have been demonstrated. Operating voltages in excess of 60 kV have been demonstrated repeatedly in these same devices and the highest operating voltage achieved was 84 kV [1].

Operation of the device at high voltage leads to a number of advantages over solid state devices. For example, in order to achieve a 100 kV operating voltage, if the device is rated for 3 kV, then standard design practice would require that at least 67 devices be placed in series. Even if PEBB and converter stacking techniques are used, the sheer number of devices required will lead to packaging, protection, control, and reliability problems. The cost of such a system will also be quite high. In addition, characteristic matching tends to be more of an issue in high voltage devices. While the problem can be solved, close tolerance matching (which is required in long stack-ups) can easily double the cost of a converter. A further problem stems from the fact that larger solid-state devices are slow. For example, a large diameter, high-voltage thyristor may turn on at less than 500 A/μs and require 500 μs or more to recover. RATVSs have been operated at over 1,000 A/μs and turn off in less than 5 μs.

Realization of a 100 kV, 10-20 kA RATVS is well within the reach of near-term technology. However, several issues remain to be resolved. The authors of this proposal know of no instance where an RATVS has been used in a DC-DC converter. Furthermore, the device must be force- or line-commutated. In addition, the RATVS has not yet been operated at the switching frequency required by the SSP application. The capability of the device to operate at very high rate of current rise and its fast turn-off mitigate this concern. In addition, the trigger system must be optimized and the device itself must be redesigned to minimize mass and volume and to operate well in space. Wear is not expected to be an issue because of the low required operating current. Wear is strictly a function of electrode geometry and Coulomb transfer.

1.1 Extension of previous RATVS and converter development

The specific RATVS upon which this proposed project is based was invented in the late 1970s by General Electric for use as an arc transfer mechanism in an interrupt switch. The device was further developed and miniaturized by the USSR as part of a laser development program. More recently, Maxwell Physics International (MPI) has been developing light-weight vacuum switches for use in a 12 GW converter for rail guns and several other high-voltage, high-current applications. In addition, The University of Texas Center for Electromechanics (UT-CEM) has extensively characterized the Russian RATVS and designed two-way ac-DC converters for very high-power alternators that employ RATVSs as the main switching elements. In addition, UT-CEM is using a bank of RATVSs as the primary power transfer switch in a very-high-velocity plasma spray system.

2 DC-DC converter circuits for space applications

This chapter gives an overview of the proposed Jones DC-DC chopper circuit [3], [4], that will utilize rod array triggered vacuum switches to interface NASA's photovoltaic DC source and transmission line to the microwave load. The Jones circuit was selected because of its proven reliability and operation with forced-commutated power electronic switches (specifically SCRs) that have essentially the same circuit properties as RATVS.

Example circuits are described, and Saber [5] simulation results are presented. The examples fit into the following three categories:

- preliminary examples with low voltage and low-to-mid power
- high voltage examples with modular one-twelfth power and full power
- an example for a proposed proof-of-concept prototype that can be built and tested at UT-CEM

2.1 NASA requirements

The DC voltage produced by NASA's large photovoltaic array in space will most likely be in the 100kV range, and at a power level of 1,000 MW. The utilization level, after the power is transmitted over some distance, is expected to be either 40 kV or 6 kV, depending on the type of microwave loads employed. Thus, DC-DC voltage conversion is essential on the load end to reduce the voltage level to a low-ripple, constant output. Weight and reliability are the most

important features of the converter. Load voltage ripple should be limited to a few percent. Parallel converters may be preferable to a single converter because of reliability and maintenance considerations.

For purposes of this study, the load voltage is assumed to be 40 kV; 6kV operation would likely require the use of a third coupled coil.

2.2. Overview of the Jones chopper circuit

The main feature of the Jones chopper circuit (fig. 2) is that it uses two switches to produce the turn-on and turn-off switching required to achieve DC-DC buck conversion with no turn-off devices. The switches are represented in the circuit diagram by SCR symbols. SCR1 is the turn-on switch. SCR2, in conjunction with capacitor C, force-commutates SCR1 off to complete the cycle. The practical duty cycle (D) range is 20% to 80%. The presence of coupled coils L_1 and L_2 (sometimes referred to as an autotransformer) measurably enhances the reliability of the circuit. Assuming relatively low ripple voltage on the load, the ratio of load voltage V_L to input voltage E_b is approximately D.

In practice, a shunt capacitor would be connected in parallel with DC source E_b to provide the ripple current, thereby permitting constant DC current to be drawn from the photovoltaic source. Another possibility to provide constant DC source current would be to reconfigure the circuit as a boost converter and use a third coupled coil to reduce the voltage appropriately.

In the chopper portion of the circuit, coupled coils L_1 and L_2, and commutation capacitor C must be properly sized. L_1 and L_2 are commonly chosen to have equal inductance values. In the load portion, smoothing elements L_f and C_f are selected to control ripple in the load voltage.

2.2.1 Design of the chopper portion of the circuit

When SCR1 is turning off, the energy stored in L_1 is transferred to commutation capacitor C. Thus, as a first approximation,

- $\frac{1}{2}L_1 I_L^2 = \frac{1}{2}CV_C^2$

where I_L is the pre-turn-off current flowing through coil L_1 (i.e., the load current), and V_C is the post-turn-off voltage across C when its current tries to reverse, causing diode D2 to open. Rewriting the above equation yields

$$\blacklozenge \quad \frac{V_C}{I_L} = \sqrt{\frac{L_1}{C}} \ . \tag{2.1}$$

During SCR1 turn-off time t_c, the voltage on C drops from V_C to zero while its current rises from zero to I_L. Thus the approximate charge deposited on C during t_c is limited to

$$\blacklozenge \quad I_L t_c = CV_C \text{, so that } t_c = \frac{CV_C}{I_L} \ .$$

Substituting (2.1) into the above equation yields

$$\blacklozenge \quad t_c = C\sqrt{\frac{L_1}{C}} = \sqrt{CL_1} \ . \tag{2.2}$$

For a 100% safety factor in turning off SCR1, t_c should be twice the turn-off time (i.e., t_q) of SCR1, or

$$\blacklozenge \quad t_c = 2t_q \ . \tag{2.3}$$

The highest operating frequency is limited by turn-off time and should not exceed

$$\blacklozenge \quad f_{\max} = \frac{1}{20t_c} = \frac{1}{40t_q} \ . \tag{2.4}$$

Now, define Q as the ratio of peak capacitor voltage V_C to input voltage E_b,

$$\blacklozenge \quad Q \equiv \frac{V_C}{E_b} \tag{2.5}$$

Q is an important design parameter since it, along with E_b, determines the voltage ratings of SCR1, SCR2, and C.

The design is completed by computing L_1 and C from the above equations. Substituting (2.5) into (2.1) and solving for $\sqrt{L_1}$ yields

$$\blacklozenge \quad \sqrt{L_1} = \frac{QE_b\sqrt{C}}{I_L} \ .$$

Likewise, from (2.2),

$$\sqrt{L_1} = \frac{t_c}{\sqrt{C}} \tag{2.6}$$

Setting the above two equations equal yields

$$\frac{QE_b\sqrt{C}}{I_L} = \frac{t_c}{\sqrt{C}}, \text{ so that C becomes}$$

$$C = \frac{t_c I_L}{QE_b} \tag{2.7}$$

Substituting (2.7) into (2.6) yields L_1 and L_2,

$$L_1 = L_2 = \frac{t_c^2 QE_b}{t_c I_L} = \frac{t_c QE_b}{I_L} \tag{2.8}$$

Summarizing, once E_b, I_L, Q, and t_q are known or chosen, then the remaining component values and ratings can be computed using (2.3), (2.7), and (2.8).

2.2.2 Design of the load portion of the circuit

The purpose of L_f and C_f is to reduce the ripple voltage on load resistor R_L. The smaller the duty cycle D, the more filtering required. L_f should be large enough so that its current is continuous for the smallest expected D and lowest expected load current I_L. This will be guaranteed if, in the worst case, the current in L_f ramps up from zero to $2I_L$ (when SCR1 is closed and diode D1 is closed), and ramps down from $2I_L$ to zero (when SCR1 is open and diode D1 is open). The ramp-up time is DT, and the ramp-down time is $(1-D)T$, where T is the converter period of operation. Examining the current ramp-down time, and *applying a safety factor of 2*, yields

$$L_f \frac{\Delta I}{2\Delta T} = \frac{0 - 2I_L}{2(1-D)T} = -V_L$$

so

$$L_f = 2V_L \frac{(1-D)T}{2I_L} = 2V_L \frac{(1-D)}{2fI_L}.$$

In situations where input voltage E_b, load voltage V_{load}, and duty cycle D are fixed, it is helpful to rewrite the above equations as

$$\blacklozenge \quad L_f = 2V_L \frac{(1-D)V_L}{2fP_L} = \frac{2V_L^2(1-D)}{2fP_L} \tag{2.9}$$

where the frequency of operation of the converter is

$$\blacklozenge \quad f = \frac{1}{T}$$

C_f should be selected so that load time constant $R_L C_f \geq \frac{5}{f}$. Rewriting in terms of input voltage and duty cycles yields

$$\blacklozenge \quad C_f = \frac{5}{R_L f} = \frac{5P_L}{V_L^2 f} \tag{2.10}$$

2.3 Preliminary examples with low voltage

2.3.1 Example #1 – Input = 1,000 V, 25 A (chopped), output = 400 V, 25 A, 10 kW; frequency = 1kHz

Consider the Jones chopper shown in figure 2 with the following specified values:

- Input voltage E_b = 1,000 V
- Load voltage V_L = 400 V
- Load power P_L = 10 kW
- SCR1 and SCR2 t_q = 20 μs
- Operating frequency 1 kHz
- Q = 1.0

The calculation steps are then

- Duty cycle $D = \frac{V_L}{E_b} = \frac{400}{1000} = 0.40$,
- From (2.3), $t_c = 2t_q = 40\mu s$,
- Load current $I_L = \frac{P_L}{V_L} = \frac{10{,}000}{400} = 25A$,

- Load resistance $R_L = \frac{V_L^2}{P_L} = \frac{400^2}{10{,}000} = 16\Omega$,
- From (2.7), $C = \frac{40 \bullet 25}{1.0 \bullet 1000}(10^{-6}) = 1.0\mu F$,
- From (2.8), $L_1 = L_2 = \frac{40 \bullet 1.0 \bullet 1000}{25}(10^{-6}) = 1600\mu H = 1.60mH$,
- From (2.9), $L_f = \frac{2 \bullet 400^2 \bullet (1-0.4)}{2 \bullet 1000 \bullet 10{,}000} = 9.6mH$,
- From (2.10), $C_f = \frac{5}{R_L f} = \frac{5P_L}{V_L^2 f} = \frac{5 \bullet 10{,}000}{400^2 \bullet 1{,}000} = 312.5\mu F$.

The solved load voltage (using Saber time step 0.1 μs) is shown in figure 3. (Note – the design procedure calls for C = 1μF, but the circuit will not solve in Saber if C > 0.5μF. This problem is believed to be due to numerical precision).

2.3.2 Scaling formulas

The above example can be scaled for other values of voltage and power. For example, let E_b^{new} , V_L^{new} , and P_L^{new} be the new input voltage, load voltage, and load power, respectively. Assuming fixed Q, f , D, and t_c , the values computed in Example 1 can readily be scaled as follows:

From (2.7)

- $C^{new} = C^{old} \bullet \frac{P_L^{new}}{P_L^{old}} \bullet \left(\frac{V_L^{old}}{V_L^{new}} \right)^2$.

From (2.8)

- $L_1^{new} = L_1^{old} \bullet \frac{P_L^{old}}{P_L^{new}} \bullet \left(\frac{V_L^{new}}{V_L^{old}} \right)^2$.

Interestingly, the product $L_1 C$ remains constant.

From (2.10) and (2.9),

- $C_f^{new} = C_f^{old} \bullet \frac{P_L^{new}}{P_L^{old}} \bullet \left(\frac{V_L^{old}}{V_L^{new}} \right)^2$.

- $L_f^{new} = L_f^{old} \bullet \frac{P_L^{old}}{P_L^{new}} \bullet \left(\frac{V_L^{new}}{V_L^{old}} \right)^2$

The product $L_f C_f$ remains constant.

If the power rises according to the square of voltage, then the component values do not change. However, their current and voltage ratings will increase.

2.3.3 Example #2 – Modification of example #1 to boost the load voltage

The circuit of example #1 can be modified to boost the load voltage by including a third winding on the autotransformer (fig. 4).

The load terms are adjusted for the new voltage, but constant power level. Compared to example #1, the load voltage is boosted approximately by the ratio $\frac{L_3}{L_1}$. The graph of load voltage is shown in figure 5.

2.3.4 Example #3 – Scaling of example #1 for input = 15kV, 10kA (chopped); output = 12 kV, 10 kA, 120 MW; frequency = 1 kHz

In this case,

- duty cycle $D = \frac{V_{load}}{E_b} = \frac{12{,}000}{15{,}000} = 0.80$

Assuming that t_q and Q are unchanged, the calculation procedure yields

- $t_c = 2t_q = 40\mu s$

- Load current $I_L = \frac{P_L}{V_L} = \frac{120 \bullet 10^6}{12 \bullet 10^3} = 10kA$ (as given)

- Load resistance $R_L = \frac{V_L^2}{P_L} = \frac{12{,}000^2}{120 \bullet 10^6} = 1.2\Omega$

- $C = \frac{40 \bullet 10^{-6} \bullet 10 \bullet 10^{3}}{1.0 \bullet 15 \bullet 10^{3}} = 26.7 \mu F$

- $L_1 = L_2 = \frac{40 \bullet 10^{-6} \bullet 1.0 \bullet 15 \bullet 10^{3}}{10 \bullet 10^{3}} = 60 \mu H$

- $L_f = \frac{2 \bullet 12{,}000^2 \bullet (1 - 0.8)}{2 \bullet 1000 \bullet 120 \bullet 10^{6}} = 0.240 mH$

- $C_{fr} = \frac{5}{R_L f} = \frac{5P_L}{V_L^2 f} = \frac{5 \bullet 100 \bullet 10^{6}}{12{,}000^2 \bullet 1{,}000} = 3472 \mu F$

The modified circuit is shown in figure 6. (Note – the design procedure calls for C = 26.7 μF, but the circuit will not solve in Saber if C > 10 μF.) The solved load voltage is shown in figure 7.

2.3.5 Example 4 – Reconfiguration of Jones chopper to construct a boost converter with low ripple source current: input = 1,000 V, 10 A (low ripple); output = 1,667 V, 6 A, 10 kW; frequency = 1 kHz

The Jones chopper has discontinuous source current. In photovoltaic applications, it is important for power tracking purposes to hold the PV current ripple to a few percent. This can be accomplished by adding a large shunt capacitor at the input of the converter to provide the ripple current, or by operating the converter as a boost converter [6].

By moving the filter inductor to the input, and moving the freewheeling diode to be in series with the load, the Jones chopper is converted to a boost converter. The circuit is shown in figure 8.

The only significant differences between the design equations of the Jones chopper and the circuit in figure 8 are that the pre-turn off current in (2.1) is now the source current (i.e., through filter inductor L_f) instead of the load current.

- $V_L = E_b \bullet \frac{1}{1 - D}$ (i.e., the standard boost equation)

in (2.9), V_L should be replaced with E_b. The calculations are now

- Duty cycle $\frac{1}{1-D} = \frac{V_L}{E_b} = \frac{1667}{1000} = 1.667$, so $D = 0.4$.

From (2.3), $t_c = 2t_q = 40\mu s$

- Load current $I_L = \frac{P_L}{V_L} = \frac{10{,}000}{1667} = 6A$,
- Load resistance $R_L = \frac{V_L^2}{P_L} = \frac{1667^2}{10{,}000} = 277.9\Omega$,
- Source current $I_S = \frac{P_L}{E_b} = \frac{10{,}000}{1000} = 10A$,
- From modified (2.7), $C = \frac{t_c I_S}{QE_b}$ $C = \frac{40 \bullet 10}{1.0 \bullet 1000}(10^{-6}) = 0.4\mu F$,
- From modified (2.8), $L_1 = L_2 = \frac{40 \bullet 1.0 \bullet 1000}{10}(10^{-6}) = 4.0mH$,
- From modified (2.9), $L_f = \frac{2 \bullet 1000^2 \bullet (1-0.4)}{2 \bullet 1000 \bullet 10{,}000} = 60mH$. Double this value to provide more smoothing on the source current, so $L_f = 120mH$
- From (2.10), $C_f = \frac{5}{R_L f} = \frac{5P_L}{V_L^2 f} = \frac{5 \bullet 10{,}000}{1667^2 \bullet 1{,}000} = 18.0\mu F$. Double this value to provide more smoothing on the output voltage, so $C_f = 36.0\mu F$.

The load voltage and source current are shown in figures 9 and 10, respectively.

2.4 High voltage examples with modular one-twelfth power and with full power converter

2.4.1 One-twelfth modular power converter suitable for paralleling

At full voltage, and one-twelfth power (i.e., 83.3MW), the load current and coil currents are approximately 2 kA, which is a desirable modular size from the point of view of the diameters of the conductors used in constructing the coupled coils. Furthermore, there are reliability and maintenance benefits in having the total system power divided among several

separate, paralleled, independent converters. For these reasons, plus the fact that the 2kA gives long life to the RATVS, this modular circuit is believed to be a good choice for NASA.

The initial design values are

- Input voltage E_b = 100kV
- Load voltage V_{load} = 40kV
- Load power P_{load} = 83.33MW
- SCR1 and SCR2 t_q = 10μs
- Operating frequency 2kHz (a more realistic rate than 1kHz for RATVS)
- Q = 1.0

Then, from equations (2.1) through (2.10),

- Duty cycle $D = \frac{V_L}{E_b} = \frac{40{,}000}{100{,}000} = 0.40$
- $t_c = 2t_q = 20\mu s$
- Load current $I_L = \frac{P_L}{V_L} = \frac{83.33 \bullet 10^6}{40 \bullet 10^3} = 2.083kA$
- Load resistance $R_L = \frac{V_L^2}{P_{lL}} = \frac{40{,}000^2}{83.33 \bullet 10^6} = 19.2\Omega$
- $C = \frac{20 \bullet 2{,}083}{1.0 \bullet 100{,}000}(10^{-6}) = 0.417\mu F$
- $L_1 = L_2 = \frac{20 \bullet 1.0 \bullet 100{,}000}{2{,}083}(10^{-6}) = 960\mu H$
- $L_F = \frac{2 \bullet 40{,}000^2 \bullet (1-0.4)}{2 \bullet 2000 \bullet 83.33 \bullet 10^6} = 5.76mH$
- $C_F = \frac{5}{R_L f} = \frac{5P_L}{V_L^2 f} = \frac{5 \bullet 83.33 \bullet 10^6}{40{,}000^2 \bullet 2{,}000} = 130\mu F$

Reasonable estimates for the resistive and inductive parasitics, plus imperfect coupling between the two coils (k = 0.9), are included in the simulation. By successively simulating the circuit with Saber, it was possible to fine tune and lower some of the inductor and capacitor values from

those computed above. Notably, L_1 and L_2 were lowered to 10μH, L_F was lowered to 3 mH, and C_F was lowered to 100 μF (fig. 11). Results are shown in figures 12 through 17.

2.4.2 Full power circuit

The schematic for a full power unit is shown in figure 18. The notable component changes compared to the one-twelfth power converter are

- the mH values of L_F, L_1, and L_2 reduce by a factor of twelve, but the corresponding current ratings increase by a factor of twelve
- the μF capacity of C_F decreases by a factor of twelve
- free wheeling diode D_{free} current increases by a factor of twelve
- RATVSs must be paralleled to increase their combined current rating to 25 kA

Except for the scale factors, the simulation graphs (though not shown here) are essentially the same as for the one-twelfth power converter.

2.5 Proposed proof-of-concept prototype

The concluding example is a prototype converter that could be built at UT-CEM and tested using existing DC power supplies. The circuit would permit the long-term testing and evaluation of RATVSs, plus the design and refinement of the coupled coils for relatively high currents. The proposed circuit, after adjustments through successive Saber simulations, is shown in figure 19. Simulation results are given in figures 20 through 25.

In addition to circuit parasitics, the 100 V forward drop of the RATVS, which is negligible at 100kV, is included here because it is substantial compared to the 500V power supply input.

3 Triggered vacuum switches

A vacuum switch is a switch that can generate and support an electrical discharge although the pressure of the environmental medium is quite low. A switch of this type typically operates with an ambient pressure no larger than 10^{-6} torr. Once the arc is established, the charge carriers necessary for the electrical current are supplied by the electrodes themselves. Under the influence of the discharge, the surfaces of the electrodes melt locally and vaporize emitting the particles needed for sustaining the discharge. Therefore, a vacuum switch is truly a metal plasma

switch since the metal electrodes emit the electrons and ions needed for the electrical discharge as well as neutral particles. A triggered vacuum switch (TVS) is one where the discharge is initiated at a specific desired time by an appropriate triggering mechanism that also provides the initial plasma density.

Electron emission is the mechanism at the basis of the electrical discharge. The residual background density of charge carriers in the inter-electrode gap is enhanced by electrons emitted from the cathode and by their ionization of the neutral particles leading to an exponential increase of charge carriers (avalanche). Thus, although both anode and cathode actively supply particles to the inter-electrode plasma, the cathode is the more active electrode and the one that requires more attention.

Vacuum switches trace their existence back to the late 1800's. Initially the interest in them was generated by their usefulness in making metallic coatings but, eventually, in the 1920's theories of electron emission from metals were worked out and the vacuum switch found more and more use in high power current switching. Until the late 1960's, however, the vacuum switch was a variant of lesser interest than the more popular gas filled switches.

A real breakthrough in the technology of vacuum switches was achieved by the research team at General Electric in the 1970's with the development of the diffused arc discharge vacuum switch. The intent was to maximize the electrode area covered by the discharge so that the discharge was kept in a diffused mode rather than constricted. This lowered the current density at the electrodes and reduced considerably electrode wear. The GE switch [1] has come to be known as the Rod Array Triggered Vacuum Switch (RATVS) and its design, with minor variations, is still dominant today. Figure 26 shows an exposed view of the internal parts of a switch of this type: the anode and cathode plates at the opposite end of the vacuum chamber are connected to several electrodes, essentially cylindrical in shape, that extend axially and are located on a circumference, so that electrodes of opposite polarity alternate. Thus, the anode and cathode of the switch form two symmetrical and identical halves. Figure 27 shows the cathode half of a switch with three cathode electrodes. Once fully assembled, the three anode electrodes complete the rod array.

Many performance features of the RATVS make the rationale for its use quite compelling:

- with proper choice of operating pressure and inter-electrode gap, the switch can be made to operate in the left branch of the Paschen curve, so that it can withstand high voltages. RATVS have been operated at several hundreds of kilovolts
- proper electrode design allows the switch to carry high currents (hundreds of kiloamps)
- recovery time is typically short, on the order of microseconds or less
- the device is quite compact and light-weight (e.g. a 25 kV, 200 kA switch is 150 mm in diameter and 203 mm in height for a total weight of 7 kg [7])

UT-CEM has had direct laboratory experience with RATVS, in particular with devices manufactured in Russia where most of the recent technological development has taken place. These RATVS are new versions of the basic GE switch and are sold in the U.S.A. by Maxwell Laboratories, Inc., under the part number TVS-40. They are rated at 25 kV, 100 kA, and 60 Hz. From this first hand experience, several points of interest have emerged which are summarized below [8].

- Switch recovery after turn-off was a function of both peak current and di/dt. Thus, successful recovery was obtained nearly 100% of the times when the peak current was below 20 kA, but only 20% of the times when peak current was above 80 kA. Also, although successful recoveries with di/dt as high as 550 A/μs were registered, nearly 100% successful recovery was achieved only when di/dt was kept below 100 A/μs
- dv/dt did not seem to play a major role at least up to values of 11 kV/μs. The addition of snubber circuits resulted in minor improvements
- Operation of the devices in parallel resulted in acceptable current sharing (less than 10% mismatch with sufficiently high anode voltage) but recovery performance was worse
- Operation in series was similar to that of the single devices
- The forward voltage drop across the switch exceeded the manufacturer's specifications, especially for short current pulses, and increased linearly with current

These performance issues have to be kept in mind for reliable operation of the RATVS. It is clear, however, from these results that, if the operation of the switches is limited to low peak currents and low di/dt values, the confidence of successful operation is high.

A more difficult issue is that of expected lifetime of the switches under continuous duty operation, like the one in our converter. The electrodes in a switch are subject to wear because of particle bombardment and intense heat. As was pointed out previously, the cathode in particular

is subject to erosion since it has to provide much of the plasma particles to sustain the discharge. The longevity of the switch, therefore, is determined by the ability of the electrodes, and especially the cathode, to withstand the demanding environment of an electrical discharge. Operation away from the constricted discharge mode but rather in a diffused discharge regime goes a long way toward lengthening the operational life of the switch. Also reducing the current density at the electrodes seems a desirable goal because it would reduce the probability of forming centers of intense melting and vaporization commonly referred to as "spots."

Experimental data for continuous operation of the RATVS are practically non-existent. Most research seems to have concentrated on low duty cycle service like current interrupters (most commercial devices), transfer switches in energy storage technology, and nuclear fusion applications. Thus research is needed to push the technology in the realm of continuous duty applications.

4 Component design for a modular DC-DC converter

The conclusions we have reached previously regarding the need to operate the RATVS at a low current density for longer lifetime suggest the design of a converter made of identical modules rated at a fraction of the total power that can be combined in parallel to provide the overall rating required. Thus, the RATVS of each module will have to handle only a fraction of the total current. This choice may be dictated also by considerations of overall system reliability and ease of maintenance.

The number of modules into which the whole converter should be subdivided is certainly negotiable, but it seems that in our case the number 12 results in a good combination of the several variables involved. Obviously, the procedure outlined can be repeated if a different number of modules is desirable. Therefore, let us proceed on the assumption that the 1 GW converter will be made up of 12 equal modules, each with the following specifications:

- 100 kV voltage standoff capability
- 2,083 A current switching
- 2 kHz operation
- 0.42 A*s per cycle
- 83.3 MW power

The detailed design of each component in the circuit of this one-twelfth scale module will now follow.

4.1 Design of triggered vacuum switches for long life

Every time the triggered vacuum switches conduct current, their electrodes are called to a very demanding application being subjected to particle bombardment and intense heat generation. As a result of this, the electrodes tend to erode and their ability to perform can eventually be impaired resulting in failure of the switch. It is important, therefore, to examine the issues that impact the projected useful lifetime of the electrodes of a switch.

Electrode erosion is normally a surface phenomenon that can be attributed to several mechanisms the most important of which are thermally driven. The heat generated within the plasma column and within the electrode itself can make the material undergo a phase change by melting it or vaporizing it. Liquid and vapor particles of the metal are then either removed, with consequent net electrode volume loss, or at least displaced, resulting in scarring of the electrode surface. Of the two electrodes the cathode is the one that erodes more and earlier, thus we will confine our attention to it.

The problem of heat generation and conduction at the electrode surface has been addressed analytically first by Belkin and Kiselev [9] under the assumption that the radial extent of the electrode surface affected (the cathode spot) is much larger than the penetration depth in the bulk of the electrode. This simplifies the problem to a one dimensional case and allows the Joule heating of the electrode to be neglected to a first order approximation (this turns out to be supported by the data for most metal electrodes of practical importance). They used the standard solution to the heat diffusion equation and, with some simplifying assumptions, derived a simple expression for the mass of molten metal M_m

- $$M_m = \frac{V_k}{3cT_m}\int_0^{t_p} |i(t)|\, dt$$

where the integral represents the total charge Q transferred to the cathode and

- V_k = cathode voltage drop (typically around 10 V for most materials)
- c = specific heat of electrode material
- T_m = melting temperature of electrode material

- t_p = time duration of the discharge pulse
- i(t) = current collected by the cathode

Of this mass a fraction k (erosion coefficient) is vaporized, thus the vaporized mass M_v is simply equal to k M_m . The same authors showed experimentally [10] that the erosion coefficient is pretty much constant for large values of Q. For small values of Q, however, k varies considerably and undergoes almost a step change at some threshold value Q_o below which it is very small and close to zero. Q_o is a function of the electrode material.

Although immediately criticized as superficial [11] and although using approximations which do seem questionable, the Belkin-Kiselev formulation has one merit: it matches the experimental evidence and allows a preliminary ranking of electrode materials in terms of their ability to resist erosion. Table 4.1, showing some potential electrode material candidates ranked in order of decreasing preference of the two significant parameters: the erosion threshold charge Q_o and the mass per unit charge M_v /Q eroded above this value.

Belkin [12] proceeded to make studies on an analog model of the cathode erosion process. The model predicted that, if the heat flux to the electrode and its duration were below certain limits, the melting of the electrode at the cathode spots remained a limited superficial phenomenon resulting in minimal erosion. This allowed him to find an empirical relationship for the onset of volume electrode melting which is reported below:

- $$\frac{q\sqrt{t_p}}{T_m\sqrt{k\rho c}} = \sqrt{\frac{\pi}{4}}$$

where q = heat flux at surface from plasma column

- k = thermal conductivity of electrode
- ρ = density of electrode material

If we equate q with the flux of Joule heat generated in the plasma in the vicinity of the electrode (ignoring other sources or sinks of heat of no interest to us here, e.g. from chemical reactions) we can write

- $$q \approx \frac{V_k i}{A}$$

where A = effective area of electrode affected by heat flux (base of plasma column). Substituting and rearranging [13], we find the condition for onset of electrode melting:

$$j^2 t_p = \frac{\pi}{4}\left(\frac{T_m\sqrt{k\rho c}}{V_k}\right)^2 = k_m$$

where $j = i/A$ = plasma current density at the base of the plasma column

- k_m = melting onset constant

A similar expression could be written for the onset of vaporization but, since the limit is higher, we do not need to concern ourselves with it here. Also, additional effects tied to skin depth heating can be neglected by us because they become significant only for very short pulse widths (few microseconds or less).

Therefore, as long as $j^2 t_p < k_m$ minimal electrode degradation is expected. If this limit is exceeded, large scale erosion takes place and it is a fast rising function of $j^2 t_p$ leading quickly to the onset of massive vaporization as well. Our goal, therefore, is to design our switch so that this limit is not reached.

This expression allows us to (1) generate an additional ranking of electrode materials in terms of their values of k_m and (2) estimate the current carrying capability of a given electrode Table 4.2 gives k_m for electrode material candidates listed in decreasing order of k_m.

It is to be noted that the Belkin formulation ignores the Joule heating within the electrode proper. If electrode bulk Joule heating is a dominant process, another criterion based on a different combination of material parameters applies [14] resulting in the ranking shown in Table 4.3, where σ is the electrical conductivity of the electrode.

Regarding the choice of the electrode material, the best present day technology seems to be a composite material of Cu in a W matrix. The W matrix improves the performance of Cu with respect to melting and vaporization and also adds mechanical strength to the otherwise rather soft copper bulk. A composite alloy of 67% W and 33% Cu seems to give the best results with erosion levels equal to one fifth that of pure Cu [15]. The addition of a small (3%) fraction of LaB_6 seems to improve erosion resistance even further [16].

An estimate of the current carrying capability of a W-Cu composite electrode gives the following results: using an average value of $k_m = 2 \times 10^{13}$ A^2s/m^4, for a 200 μs pulse width, we

calculate a current density of $j = \text{sqrt}(2 \times 10^{13}/.0002) = 3.2 \times 10^{8}$ A/m^2, which for a current of 2,083 A results in an electrode area of $2083/(3.2 \times 10^{8}) = 6.5 \times 10^{-6}$ m^2 = .065 cm^2. Even using a factor of 5 to account for an effective area coverage of the electrode, because the plasma column breaks into filaments (as suggested in [13]), this gives an electrode area of 0.33 cm^2. This is the minimum area necessary for carrying the current of 2,083 A for one shot without incurring in excessive electrode melting. It is rather small, which is encouraging. In order to repeat the same current pulse every 500 μs we must examine more closely the additional demands on our electrodes.

Let us estimate the thermal performance of a rod-array switch of the type we are planning to use. Assuming twelve cylindrical rods for the cathode with H = 20 cm height and D = 2.5 cm diameter, the effective area of the cathode plasma column is approximately

$$A = 12 \cdot \frac{2}{3} \pi \, DH \frac{1}{5} = 251 \, cm^2 = .0251 \, m^2$$

where we have also included the safety factor of 5 mentioned above. The RMS power flow input to the cathode is $Q_{RMS} = V_k * i * \text{sqrt}(0.4) = 10 * 2083 * \text{sqrt}(0.4) = 13.2$ KW. At steady state this is the power that also must be radiated into space to keep constant temperature at the electrode. With σ = Stefan-Boltzmann constant, ε = surface emissivity assumed to be about 0.8, T_0 = ambient temperature assumed to be 233°K, and with the radiating area A_r assumed to be equal to ten times the effective electrode area, to account for possible radiating fins extending below the electrode plate, we get for the radiating surface temperature T_1 the value

$$T_1 = \left(\frac{Q_{RMS}}{A_r \varepsilon \sigma} + T_0^4 \right)^{\frac{1}{4}} = \left(\frac{13200}{10 \cdot .0251 \cdot .8 \cdot 5.67 \cdot 10^{-8}} + 233^4 \right)^{\frac{1}{4}} = 1038 \ ^{o}K$$

This value is very close to the melting point of Cu and is obviously unacceptable. Therefore, the electrode must be cooled with external means. If the rods are made hollow with an inside diameter of d = 1.5 cm to allow for the passage of a cooling fluid at a temperature of 10°C, for example, the temperature of the inside wall of the electrode will be approximately

$$T_1 = \frac{D}{d} \frac{Q}{Ah} + T_w = \frac{2.5}{1.5} \frac{13200}{.0251 \cdot 10000} + 10 = 97 \ ^{o}C$$

and that of the outside wall will be

- $T_2 = T_1 + \frac{Q_{RMS}}{A}\frac{D}{k}\ln\left(\frac{D}{d}\right) = 97 + \frac{13200}{.0251}\frac{.025}{386}\ln\left(\frac{2.5}{1.5}\right) = 115\ ^{o}C$

This calculation does not pretend to be more than a ballpark estimate of the order of magnitude of the temperatures involved. Its intent is to establish that, with the choice of a suitable coolant (e.g. NH_3) at an appropriate flow rate and pressure, it should be feasible to keep the electrodes at a reasonable temperature and keep their erosion to a minimum.

As a double check on our design, we can see how our switch compares to the onset of large scale electrode melting:

- $j^2 t_p = \left(\frac{2083}{.0251}\right)^2 .0002 = 1.38 \cdot 10^6 << 2 \cdot 10^{13}\ \mathrm{A^2 s/m^4} = k_m$

The conceptual design of an electrode rod with forced convection cooling is shown in figure 28.

The estimate above was based on a hypothetical switch with twelve cathode rods. This switch, of course, can also be realized with the parallel operation of multiple switches with fewer rods, for example, four switches with three rods each. These switches will be able to be operated continuously at the duty cycle specified with minimal erosion at the cathode electrode rods.

The actual calculation of electrode life is not possible at present for lack of data. Belkin himself seems to imply that electrode life should not be a concern if the k_m limit is not exceeded. Quoting directly from him [12]:

> In that range of q*sqrt(t_p) values, one can expect that the specific life will not depend on the discharge time. The lack of time dependence for life with small q*sqrt(t_p) has been confirmed experimentally.

Unfortunately no detail is given for the experimental verification mentioned. Since the Belkin paper, no additional detail has surfaced in the literature that could shed light on this issue. Reference [17] mentions expressly "spotless cathode operation" as an item receiving attention in the last 25 years but does not elaborate further and concentrates on the progress made in the experimental and theoretical description of the cathode spots. The lack of data is believed to be more the result of the fact that commercial interests in the use of vacuum switches have been concentrated in the area of light duty cycles (e.g. current interrupters, energy storage switching, nuclear fusion) than of difficulty in performing the research.

Another option available for the design of electrodes with long life is given by copper electrodes clad with tungsten. In this case, the tungsten outer cover is best for handling the

electrode erosion, which is a surface phenomenon, and the copper bulk is best for reducing the Joule losses, which is a volume phenomenon.

Normally, anode erosion would also be of concern but it occurs at higher stress levels than cathode erosion. Thus, if we are successful in minimizing cathode erosion, anode erosion will also be minimized.

Another item of great importance for the lifetime of an RATVS is its trigger mechanism. This is realized most commonly as a small electrode embedded in the cathode electrode and separated from it by a dielectric. This trigger electrode is pulsed with a medium voltage spike, typically 1-5 KV in magnitude and positive with respect to the cathode, so that a small discharge is initiated between itself and the cathode. This discharge provides sufficient plasma density that the voltage across the main gap breaks it down and the main current conduction starts in the switch. Conduction will continue until current across the main gap drops to zero. Obviously, it is important that the trigger maintain its capability if we want reliable triggering of the switch.

Three items are of interest in regard to the lifetime of the trigger mechanism. First of all, the trigger electrode and the switch's cathode electrode form the anode-cathode pair of a mini-switch, thus all that has been said for the electrode erosion of the main switch can be repeated here. If the cathode is designed to minimize erosion during the conduction across the main gap, it will certainly be sufficient to avoid erosion during the conduction of the smaller trigger current. It is important, however, to make sure that the trigger electrode is designed so that itself operates in a diffused discharge mode. This is insured by proper design of the geometry of the trigger electrode.

The second item to consider is the longevity of the dielectric interposed between the trigger electrode and the cathode. This dielectric degrades under the action of the trigger arc as well as of the main discharge if it is exposed to it.

Thirdly, the trigger mechanism must be shielded from the debris that results from the main arc otherwise it may short out to the cathode.

Alternatives to using a smaller vacuum switch as the trigger for the main switch exist but add complexity to what is otherwise a very simple device. For example, optical triggering by means of laser light is a possible option, albeit more complex.

An additional item regarding the trigger device must be considered, although it is not related directly to the trigger's lifetime but rather to that of the main switch electrodes. The main discharge starts in the proximity of the trigger electrode because that is where the initial plasma density is generated. Thus, it is important to locate the trigger electrode so that a diffused discharge is favored from the start, avoiding a constricted discharge even if only a transient one [18]. One way to accomplish this is described in [19].

Therefore, we can conclude that appropriate means to minimize cathode erosion and trigger degradation have been identified and can be implemented so that the lifetime of the vacuum switches should not limit severely the operation of the DC-DC converter.

4.2 Design of the filter inductor and of the autotransformer

The design procedure used for the filter inductor and for the autotransformer is the one given by Grover [20]. Several optimization procedures can be followed with special attention given to one or two (but probably not all four) of the following variables:

- weight
- physical size
- energy loss
- cooling needs

A preliminary design optimizing the weight and keeping the current density below 170 A/cm^2 (thus imposing a condition on maximum energy loss) yields the data shown in Table 4.4. Additional details can be obtained from figures 29 and 30.

Obviously different variations are possible and the designs above give just an indication of what can be expected.

5 Potential technological developments

5.1 The rod array triggered vacuum switch

Several possible developments can be foreseen in the design of the RATVS that would make it a more reliable and robust device. Many options have already been discussed previously in the section on the design of a one-twelfth sized converter. Below is a summary with few additional comments.

- optimized electrode geometry. It is not a foregone conclusion that a cylindrical electrode geometry, or possibly a conical section with a small slanting angle is the best one. Recent developments seem to favor a trapezoidal electrode cross section [21]
- advances in electrode material
- improved trigger design
- alternative triggering mechanisms
- optimized electrode cooling

A theoretical projection for the lifetime of an RATVS will remain a difficult task especially because the experimental data in the operational regime of interest to us are scattered or non-existent. Cautious extrapolations of existing data on copper electrodes with some of the design improvements described previously lead to an expected lifetime of 300-400 hours for RATVS used in our converter. For W-Cu(LaB_6) electrodes this time could be extended by a factor between 5 and 10 giving a projected lifetime window of 1,300 to 4,000 hr for the RATVS in our converter ([14], [15], and [16]) . All this can be achieved pretty much with present day technology and experimental information.

One item to keep in mind is that when we talk about RATVS lifetime we are not necessarily addressing a catastrophic phenomenon that happens suddenly at one point in time after which the RATVS is inoperable. The only mechanism of this type in an RATVS is the triggering. Electrode erosion instead results in a progressive reduction of performance and only in extreme cases leads to sudden failure. Thus, the RATVS is a fairly robust and tolerant device that affords some flexibility in maintenance procedures.

5.2 The filter inductor and the autotransformer

Design improvement in this area can be anticipated as a result of the following:

- smaller inductance values resulting from a more optimized circuit design
- more in-depth optimization of the inductor designs per se
- optimization of the electrical, thermal, and mechanical functions resulting from experience gained at the Center for Electromechanics of the University of Texas at Austin in other programs (e.g. cooling techniques from the Electric Gun program, composite material containment from the Electric Gun and NASA Flywheel Battery programs)

A weight reduction of 30-50% can reasonably be expected based on the items above.

6 Summary and Recommendations

1. The design of an RATVS-based DC-DC converter is feasible and robust
2. System mass with present-day technology is approximately 20 T
3. With modest design optimization and technical development a mass reduction of 30 to 50% is projected
4. RATVS life is an issue that must be addressed. Feasible solutions have been identified and the risk of their implementation is moderate.
5. The construction and life-testing of de-mountable RATVS with extended lifetime should be the next step in the development of the converter. These devices will incorporate the improvements in material, cooling, and triggering that have been discussed above. It will be possible to make projections from these tests on reliability and maintenance requirements of the switches.
6. In parallel with item 5, it will be worthwhile to investigate the possibility of operating in space the RATVS in an "open bottle" configuration (no enclosure). This would allow the direct replacement of the cathode simplifying maintenance.
7. A proof-of-principle converter incorporating RATVS should be designed, built, and tested. The Center for Electromechanics has in place the infrastructure and equipment to test one such converter designed for 500 V, 1500 A, 2 KHz. Since issues associated with current are crucial insofar as switch lifetime is concerned, more so than voltage, this converter will be very useful in assessing the effectiveness of the RATVS design (the switches would be tested at ~75% rated current).
8. Proceed with the detailed design of a full-scale 100 kV – 40 kV, 25 kA, 1 GW, 2 kHz RATVS converter to determine overall system performance, size, weight, reliability, and manufacturability.

REFERENCES

1. JA Rich, et al. (General Electric Co.), *Development of a high-power vacuum interrupter*, EPRI Report EL-1895, Electric Power Research Institute, Palo Alto, CA, 1981.
2. J. A. Pappas, et al., *Characterization of triggered vacuum gaps for high-current operation*, IEEE Transactions on Magnetics, vol 35, no. 1, January 1999.
3. SCR Manual, Sixth Edition, General Electric, Prentice-Hall, Inc., Englewood Cliffs, NJ, 1979.
4. S. K. Datta, Power Electronics and Controls, Reston Publishing Company, Inc., Reston, VA, 1985.
5. Getting Started with SaberDesigner, Analogy, Inc. (now Avant! Corporation), Beaverton, OR, 1999.
6. N. Mohan, T. M. Undeland and W. P. Robbins, Power Electronics – Converters, Applications, and Design, John Wiley & Sons, Inc., New York, 1995.
7. D. F. Alferov, V. P. Ivanov, and V. A. Sidorov, *High-current vacuum switching devices for power energy storages*, IEEE Transactions on Magnetics, vol. 35, no. 1, p. 323-327, January 1999.
8. J. A. Pappas, S. P. Pish, and M. J. Salinas: *Characterization of triggered vacuum switches for high current operation*, Ninth EML Symposium, Edinburgh, Scotland, May 1998.
9. G. S. Belkin and V. Ya. Kiselev, *Electrode erosion in pulsed high-current discharges*, Sov. Phys. – Tech. Phys., vol. 11, no. 2, p. 280-283, August 1966.
10. G. S. Belkin and V. Ya. Kiselev, *Influence of electrode material on erosion at high currents*, Sov. Phys. – Tech. Phys., vol. 12, no. 5, p. 702-703, November 1967.
11. K. K. Namitokov, *Electrode erosion in high current pulsed discharges*, Sov. Phys. – Tech. Phys., vol. 12, no. 5, p. 714-716, November 1967.
12. G. S. Belkin, *Dependence of electrode erosion on heat flux and duration of current flow*, Sov. Phys. – Tech. Phys., vol. 15, no. 7, p. 1167-1170, January 1971.
13. W. C. Nunnally and A. L. Donaldson, "Self Breakdown Gaps," Sect. 3a of Gas Discharge Closing Switches, G. Schaefer, M Kristiansen, and A. Guenther Editors, Plenum Press, New York 1990.
14. A. L. Donaldson, "Lifetime Considerations," Sect. 5b of Gas Discharge Closing Switches, G. Schaefer, M Kristiansen, and A. Guenther, editors, Plenum Press, New York, 1990.
15. A. L. Donaldson, T. G. Engel, and M. Kristiansen, *State-of-the-art insulator and electrode materials for use in high current, high energy switching*, IEEE Transactions on Magnetics, vol. 25, no. 1, p. 138-141, January 1989.
16. F. M. Lehr and M. Kristiansen, *Electrode erosion from high current moving arcs*, IEEE Transactions on Plasma Science, vol. 17, no. 5, p. 811-817, October 1989.
17. R. L. Boxman, S. Goldsmith, and A. Greenwood, *Twenty-five years of progress in vacuum arc research and utilization*, IEEE Transactions on Plasma Science, vol. 25, no. 6, p. 1174-1186, December 1997.
18. D. F. Alferov and V. A. Sidorov, *High-current vacuum arc evolution in a six-gap rod electrode system*, IEEE Nineteenth International Symposium on Discharges and Electrical Insulation in Vacuum, vol. 1, p. 319-322, Xi'an, 2000.
19. T. Warren, J. Dickens, A. Neuber, M. Kristiansen, G. Frazier and I. R. McNab, *Development of improved triggered vacuum switches*, Twelfth IEEE International Pulsed Power Conference, p. 1264-1267, June 1999.
20. F. W. Grover, Inductance Calculations, Instrument Society of America 1973.
21. D. F. Alferov, N. I. Korobova and V. A. Sidorov, *The burning voltage of a high-current vacuum arc in a six-gap rod electrode system*, IEEE Transactions on Plasma Science, vol. 25, no. 4, p. 586-592, August 1997.

Table 1. Electrode candidate materials in order of initial preference

Material	Q_o [C]	M_v/Q [mg/C]
Ti	35	2.6
Mo	33	3.0
Cu	15	3.2
(W: no data)		

Table 2. Electrode candidate materials in order of k_m

Material	k_m (x 10^{13} A^2s/m^4)
W	3.82
Mo	1.70
Cu	1.22
Ti	0.31

Table 3. Electrode candidate materials in order of contuctivity

Material	$\sigma\sqrt{\rho c T_m}$ (x 10^{12} $J^{1/2}/\Omega/m^{5/2}$)
Cu	3.5
W	2.3
Mo	1.5
Ti	0.5

Table 4. Preliminary design specifications

	Filter Inductor	Autotransformer Primary	Autotransformer Secondary
Inductance	3 mH	10 μH	10 μH
Resistance at 130 °C	8.9 mΩ	0.3 mΩ	0.3 mΩ
Rated current	2,083 A	2,083 A	2,083 A
Loss at 130 °C	38.5 kW	1.3 kW	1.3 kW
Conductor weight	741 cg	26 kg	26 kg
Expected temperature rise	90°C	60°C	30°C

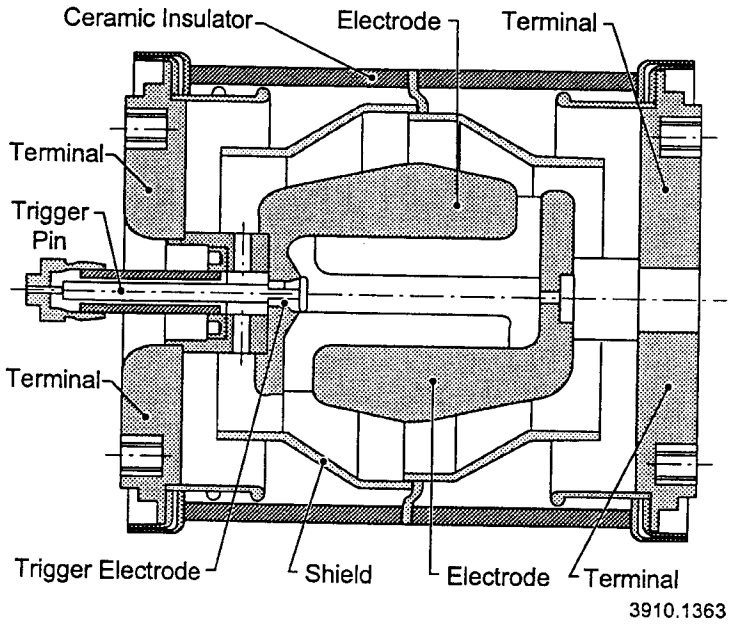

Figure 1. Commercially-available RATVS

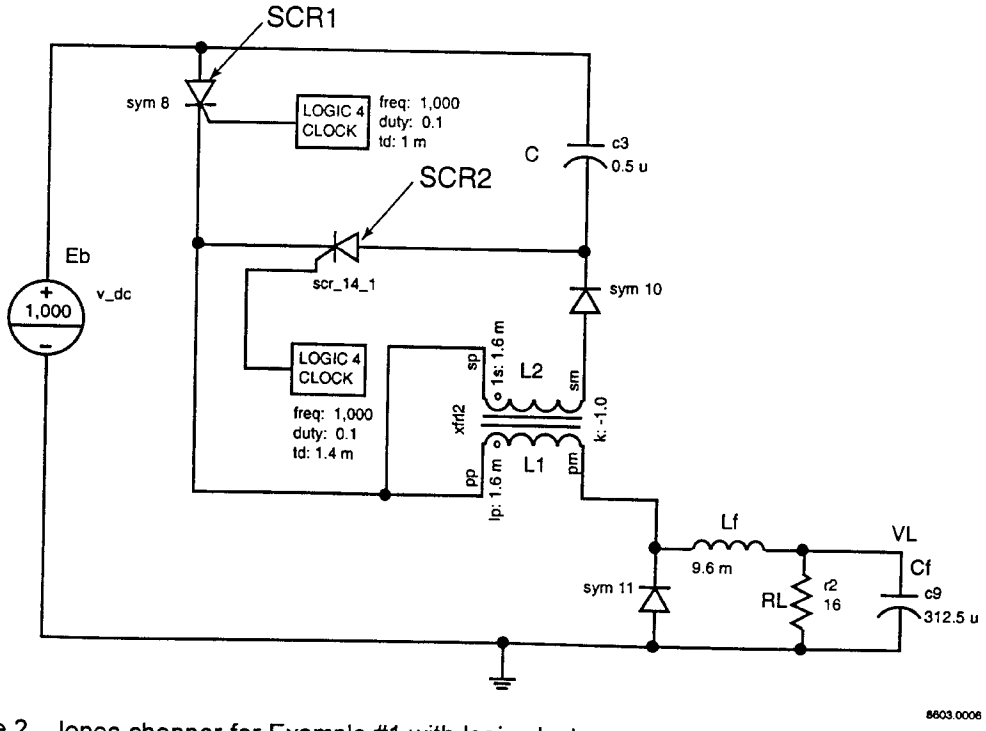

Figure 2. Jones chopper for Example #1 with logic clocks operating at 1 kHz and duty cycle 0.40
(Note: the coefficient of coupling k in the coupled coils is negative to reverse the dot polarity of one of the windings)

NASA/CR—2002-211562 28

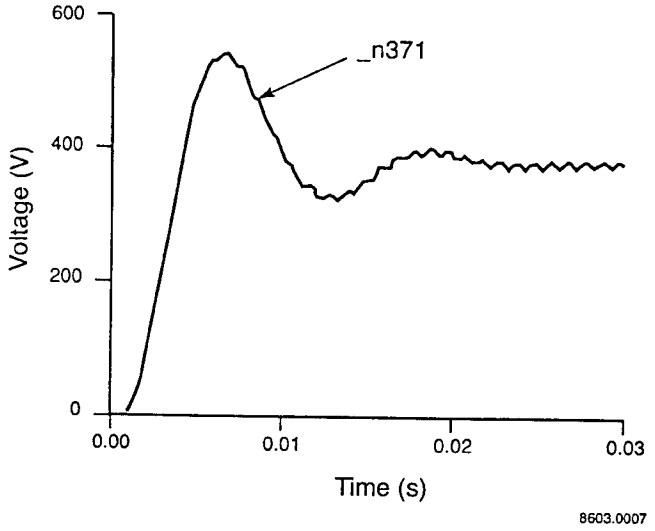

Figure 3. Load voltage for 10 kW Jones chopper in figure 2

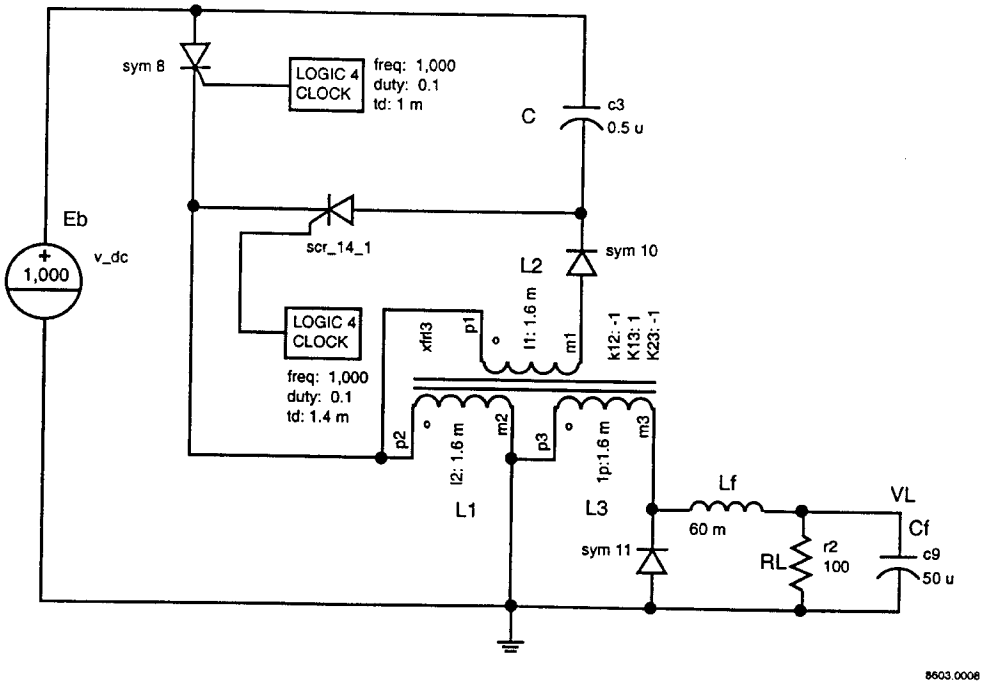

Figure 4. Jones chopper modified with booster transformer

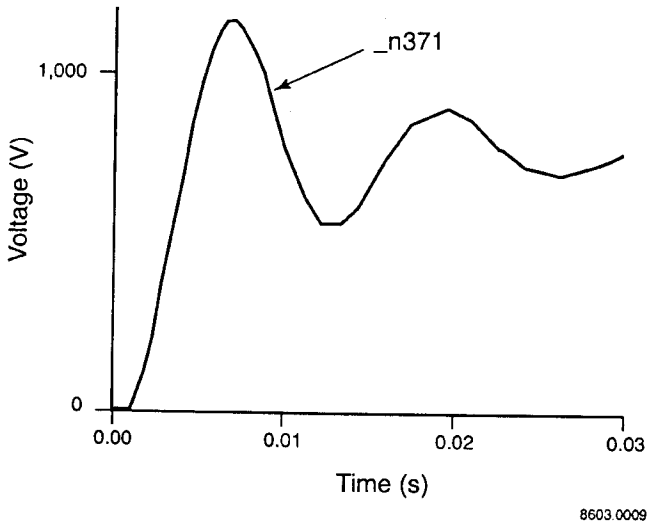

Figure 5. Load voltage for 10 kW Jones chopper in figure 4

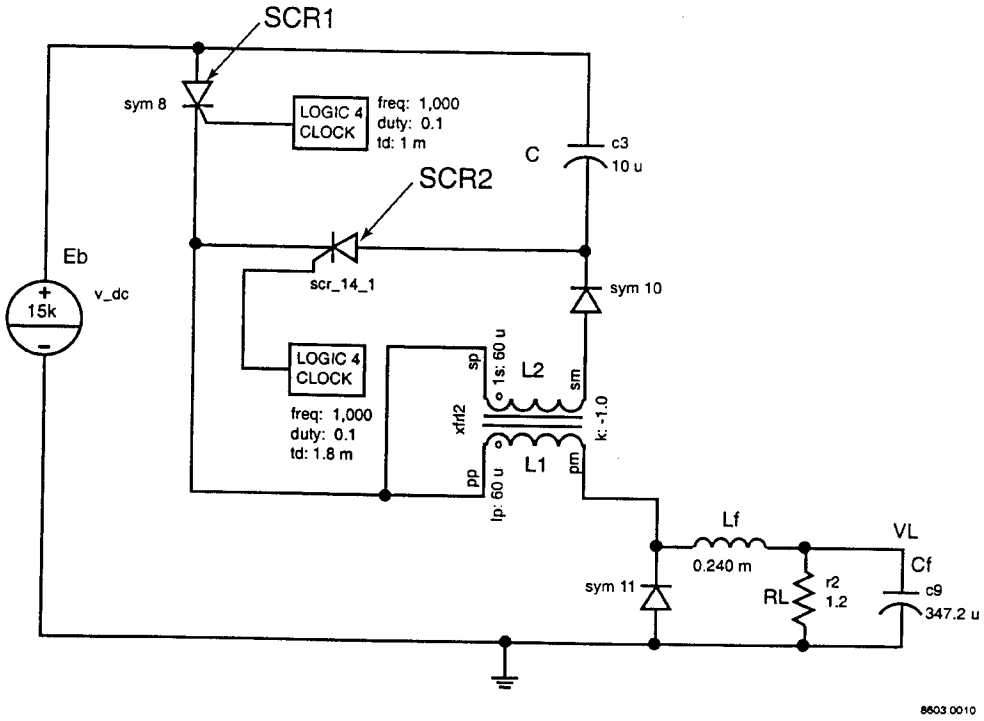

Figure 6. 100 MW Jones chopper

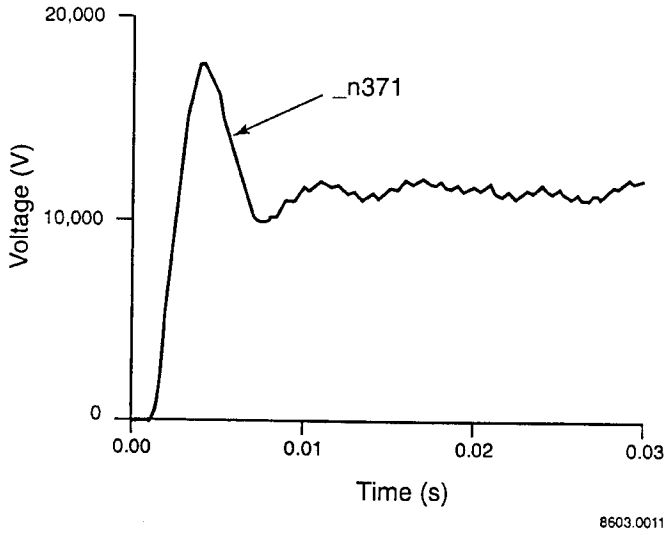

Figure 7. Load voltage for 100 MW Jones chopper of figure 6

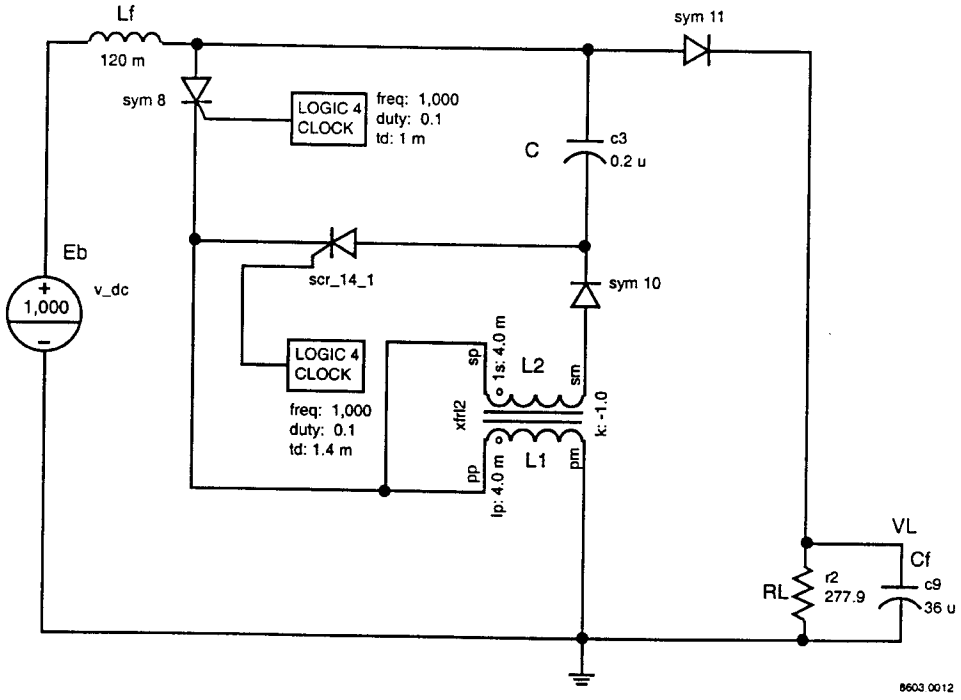

Figure 8. 10 kW Jones chopper, modified to operate as a boost converter

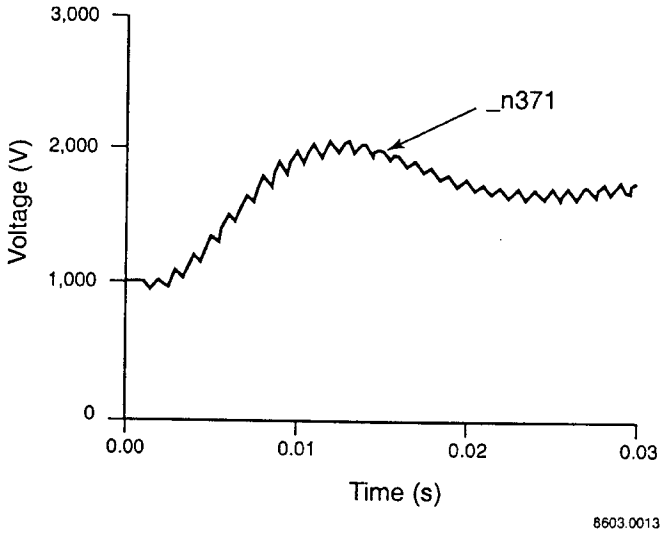

Figure 9. Load voltage for 10 kW Jones chopper-booster of figure 8

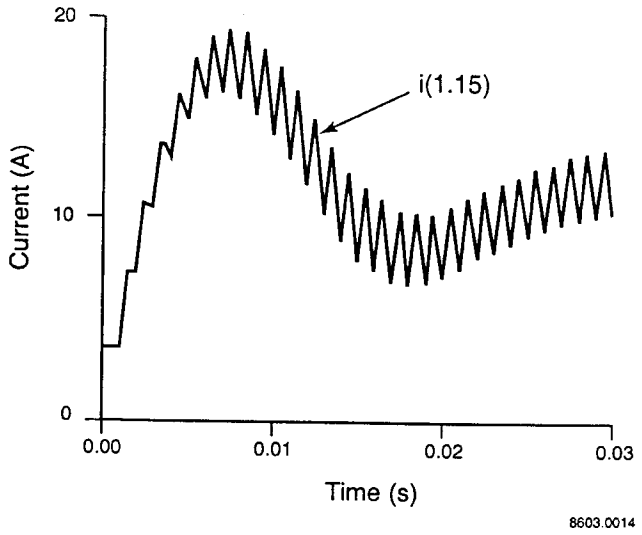

Figure 10. Source current for 10 kW Jones chopper-booster of figure 8

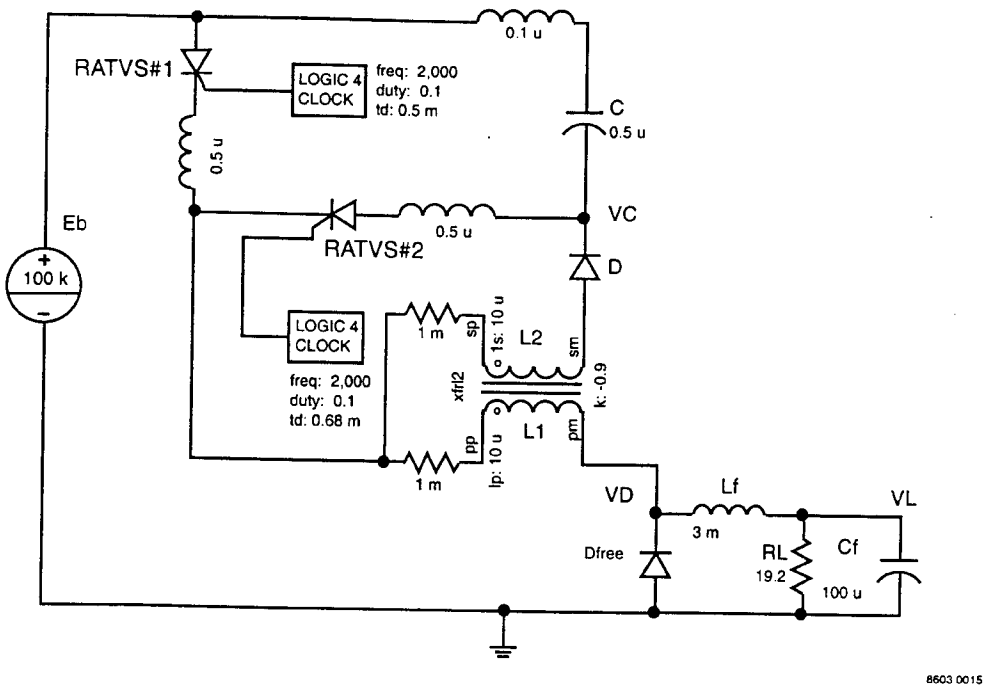

Figure 11. One-twelfth modular power converter suitable for paralleling (output 40 kV, 2,083 A, 83.3 MW)

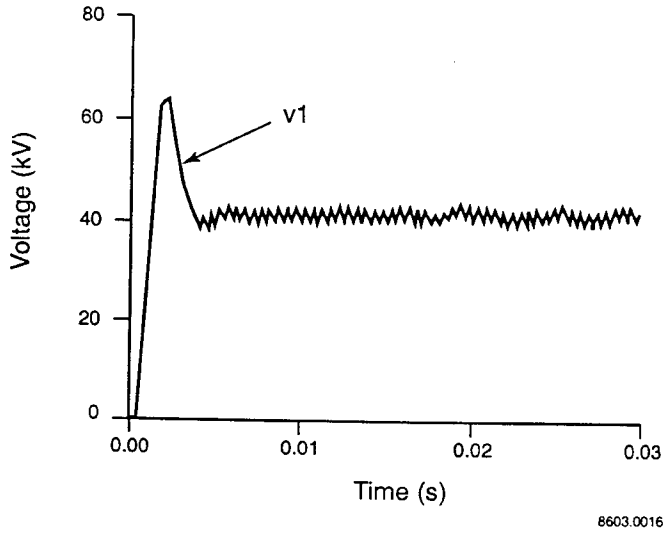

Figure 12. Load voltage for one-twelfth power converter (entire simulation)

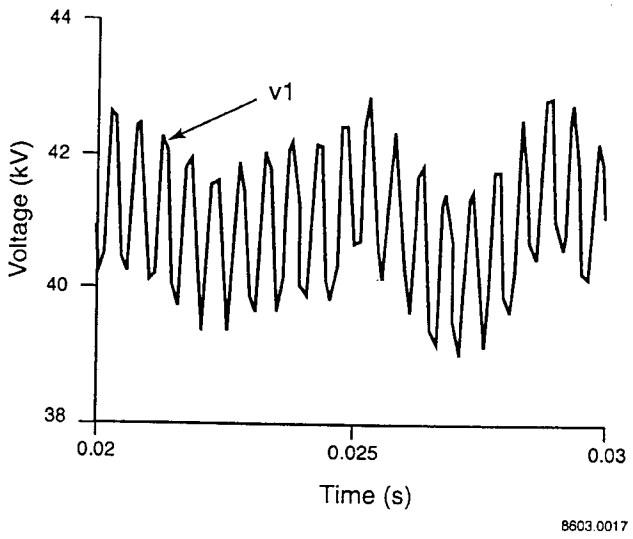

Figure 13. Load voltage for one-twelfth power converter (zoom-in of steady-state region)

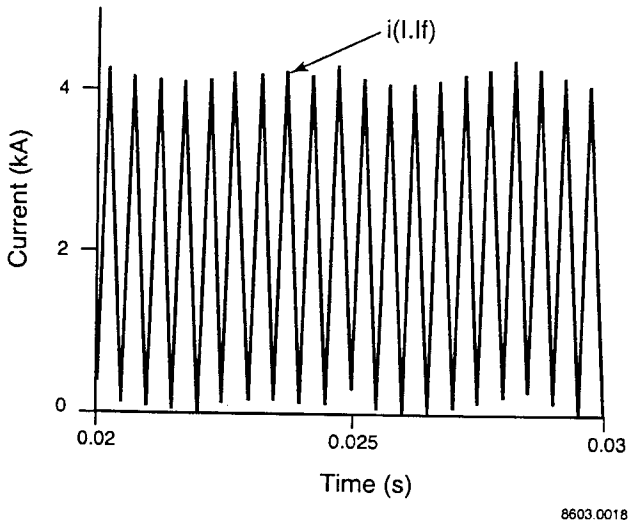

Figure 14. Filter inductor L_F current (zoom-in of steady-state region)

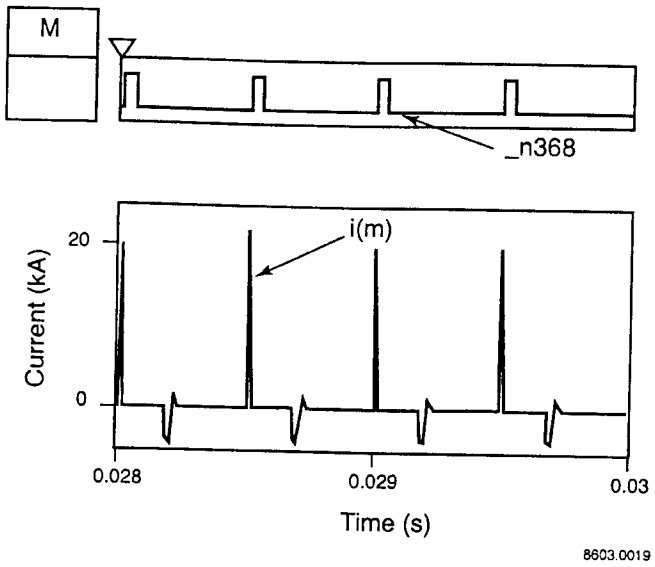

Figure 15. RATVS#1 firing pulse, and commutating capacitor C current (zoom-In of steady-state region)

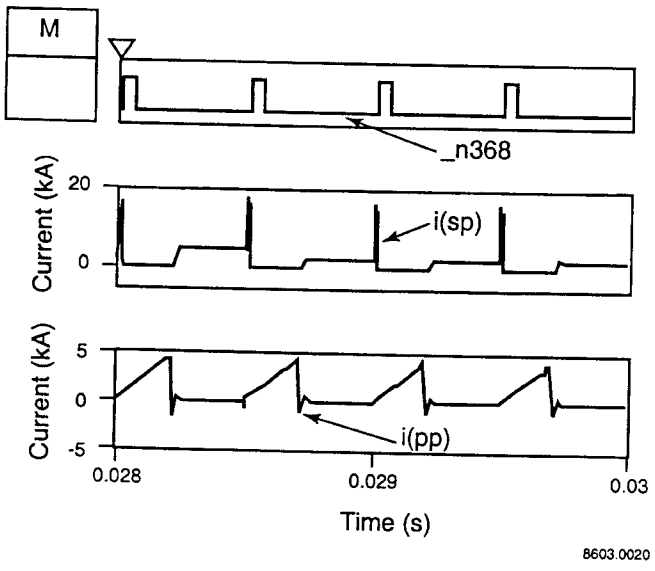

Figure 16. RATVS#1 firing pulse and coupled coil currents (left to right) (zoom-in of steady-state region)

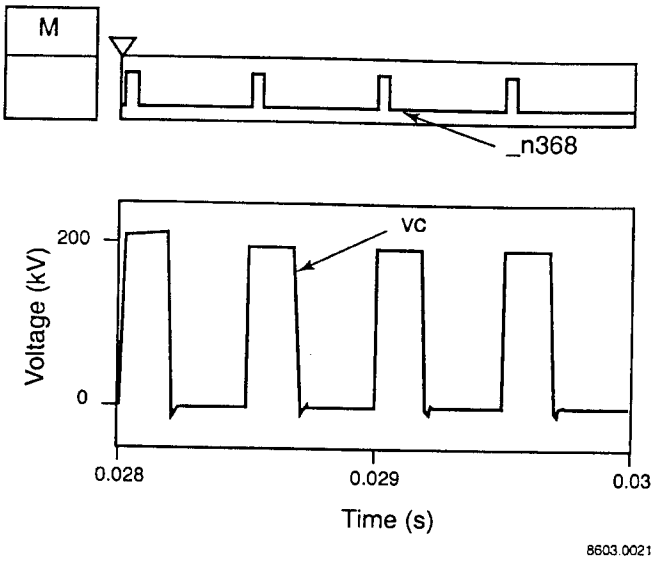

Figure 17. RATVS#1 firing pulse and commutating capacitor C voltage (zoom-in of steady-state region)

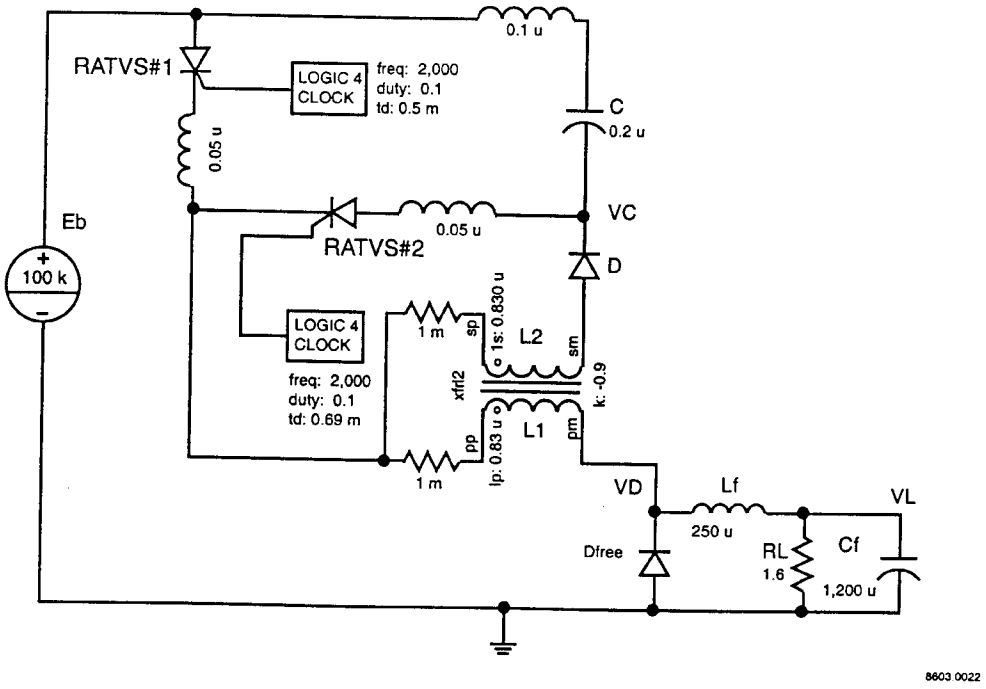

Figure 18. Full power converter(output 40 kV, 25 kA, 1,000 MW)

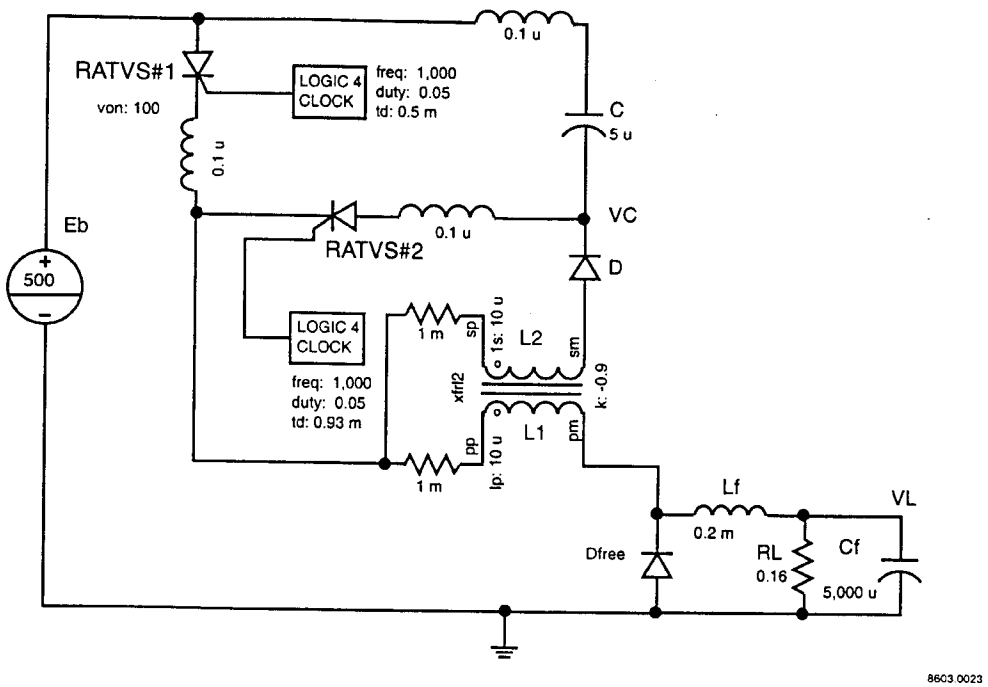

Figure 19. Proposed proof of concept prototype

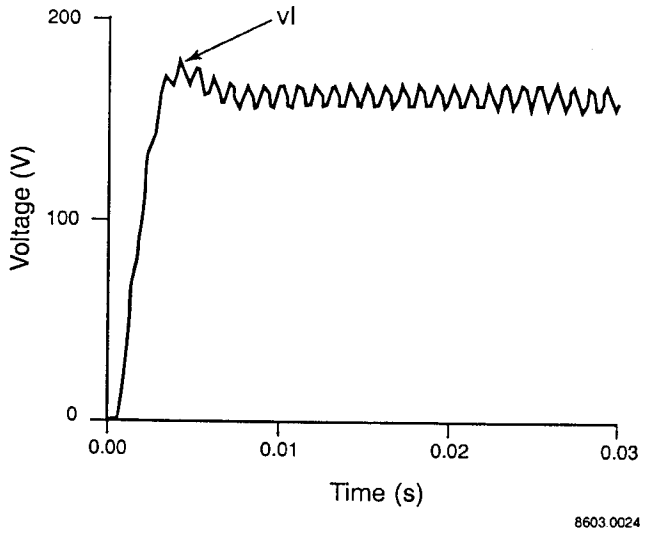

Figure 20. Load voltage for proof of concept prototype (entire simulation)

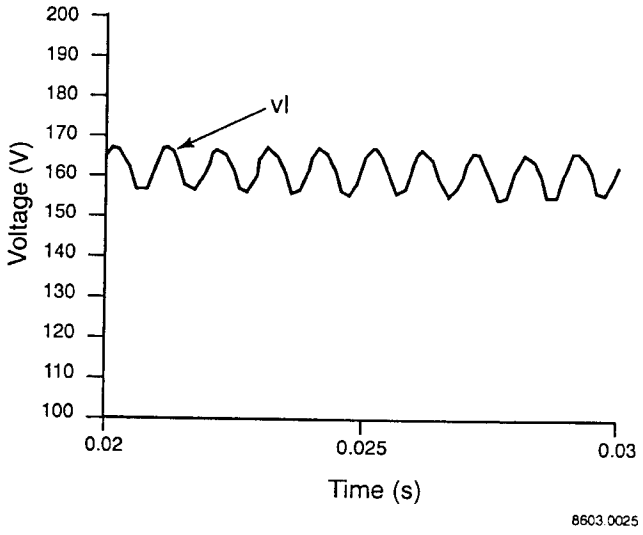

Figure 21. Load voltage for proof of concept prototype (zoom-in of steady-state region)

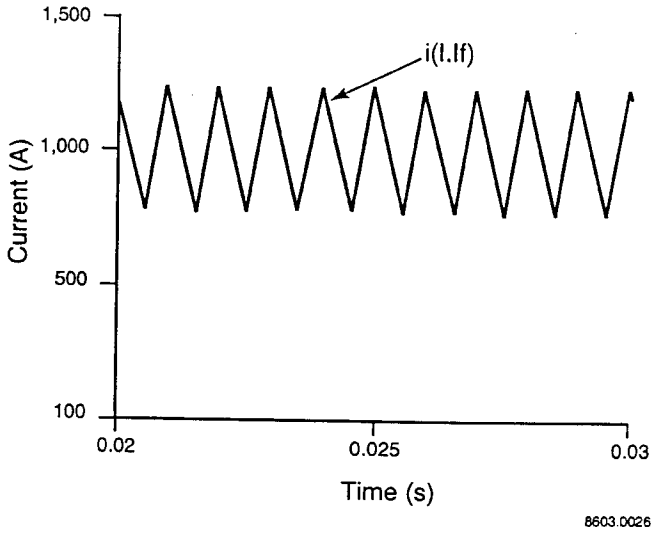

Figure 22. Filter inductor L_F current (zoom-in of steady-state region)

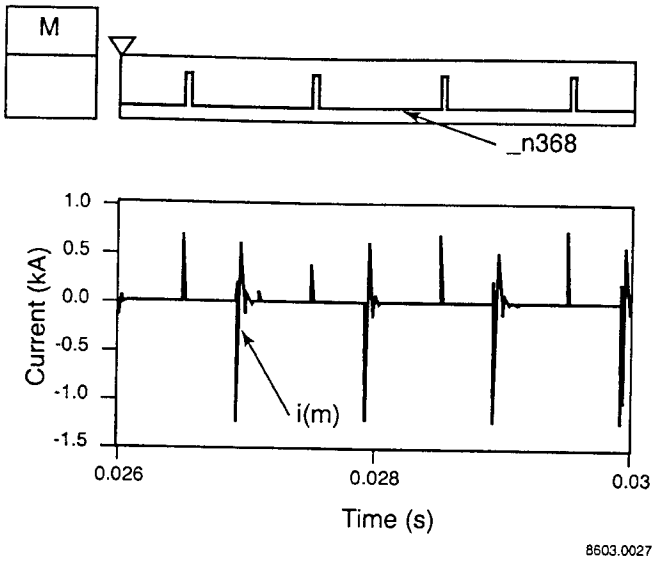

Figure 23. RATVS#1 firing pulse, and commutating capacitor C current (zoom-in of steady-state region)

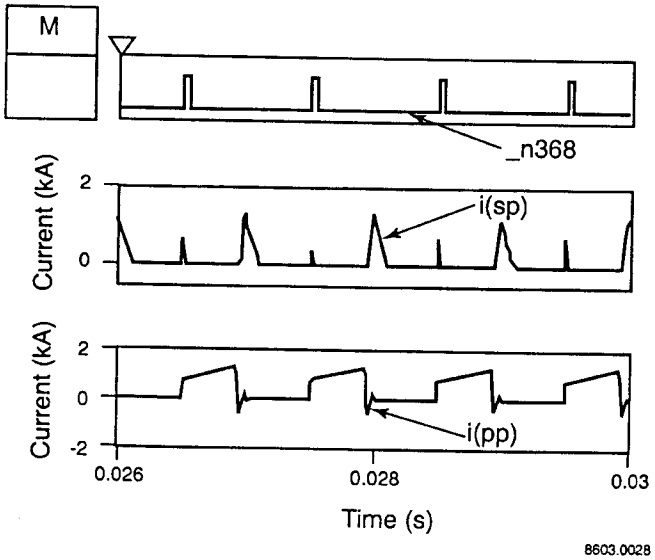

Figure 24. RATVS#1 firing pulse and coupled coil currents (left to right) (zoom-in of steady-state region)

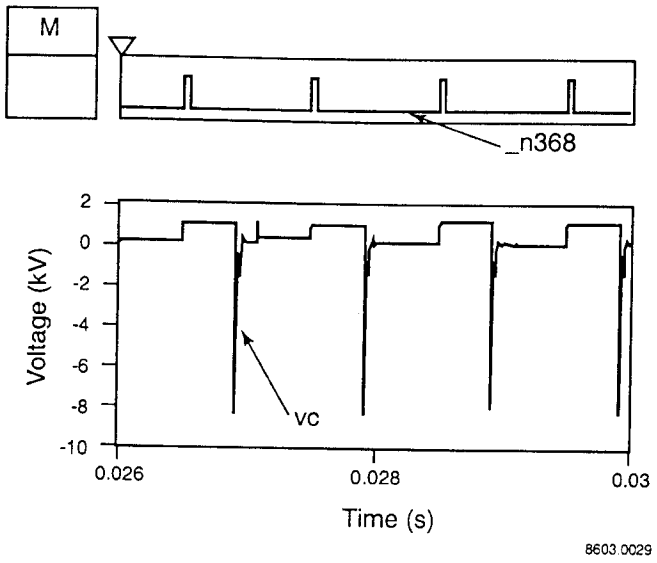

Figure 25. RATVS#1 firing pulse and commutating capacitor C voltage (zoom-in of steady-state region)

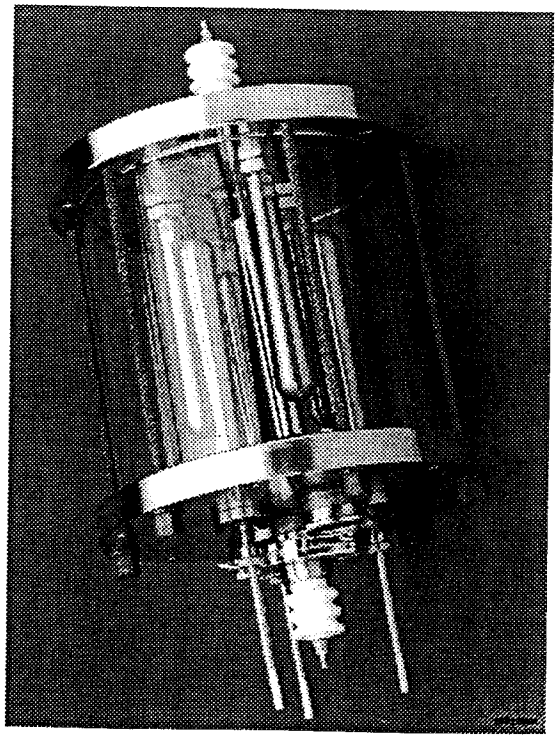

Figure 26. Open view of a rod array triggered vacuum switch

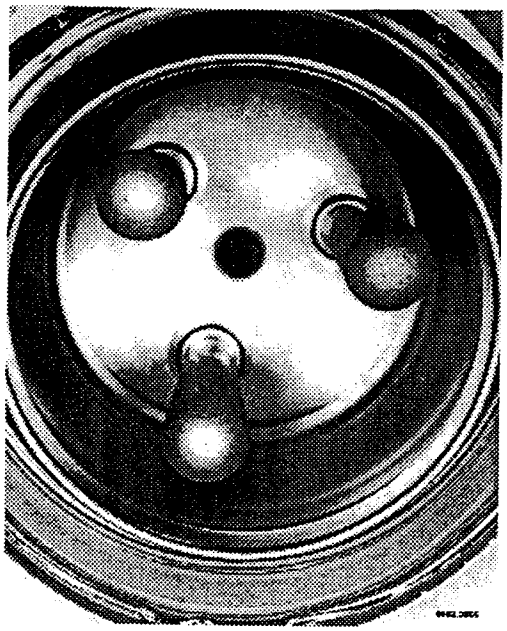

Figure 27. The cathode half of a six electrode RATVS (from [1])

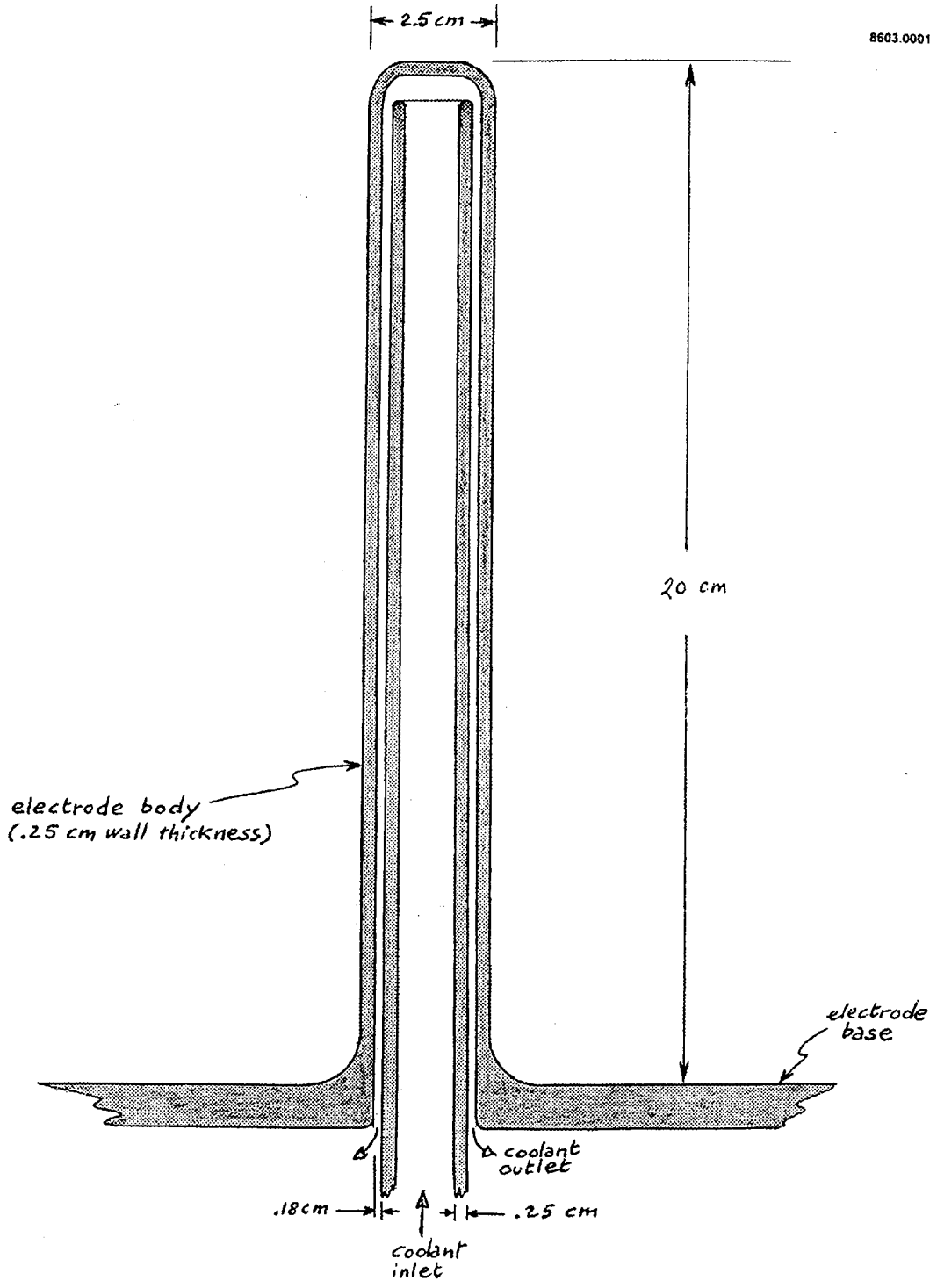

Figure 28. Conceptual design of the rod of an electrode with forced convection cooling

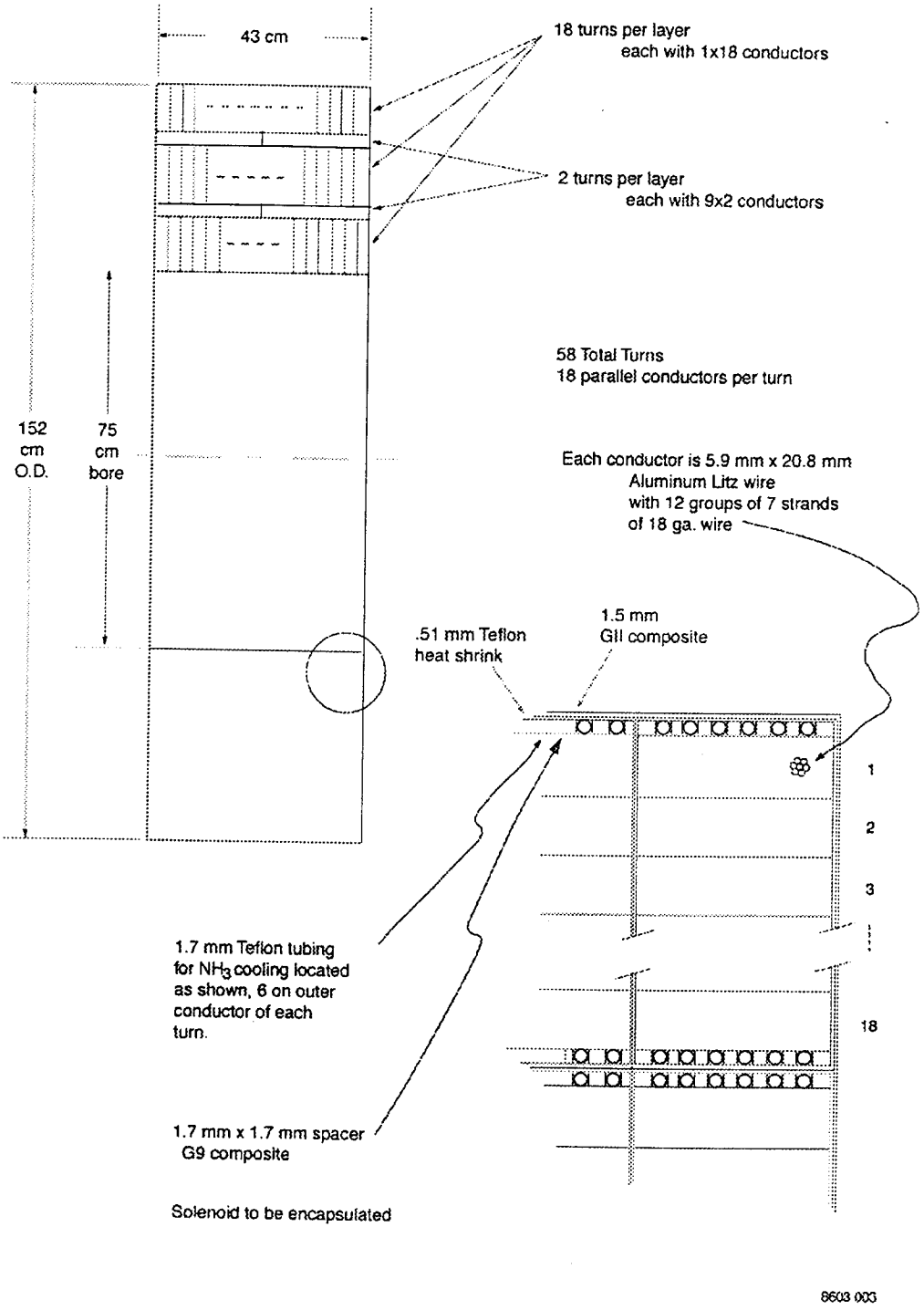

Figure 29. Filter inductor

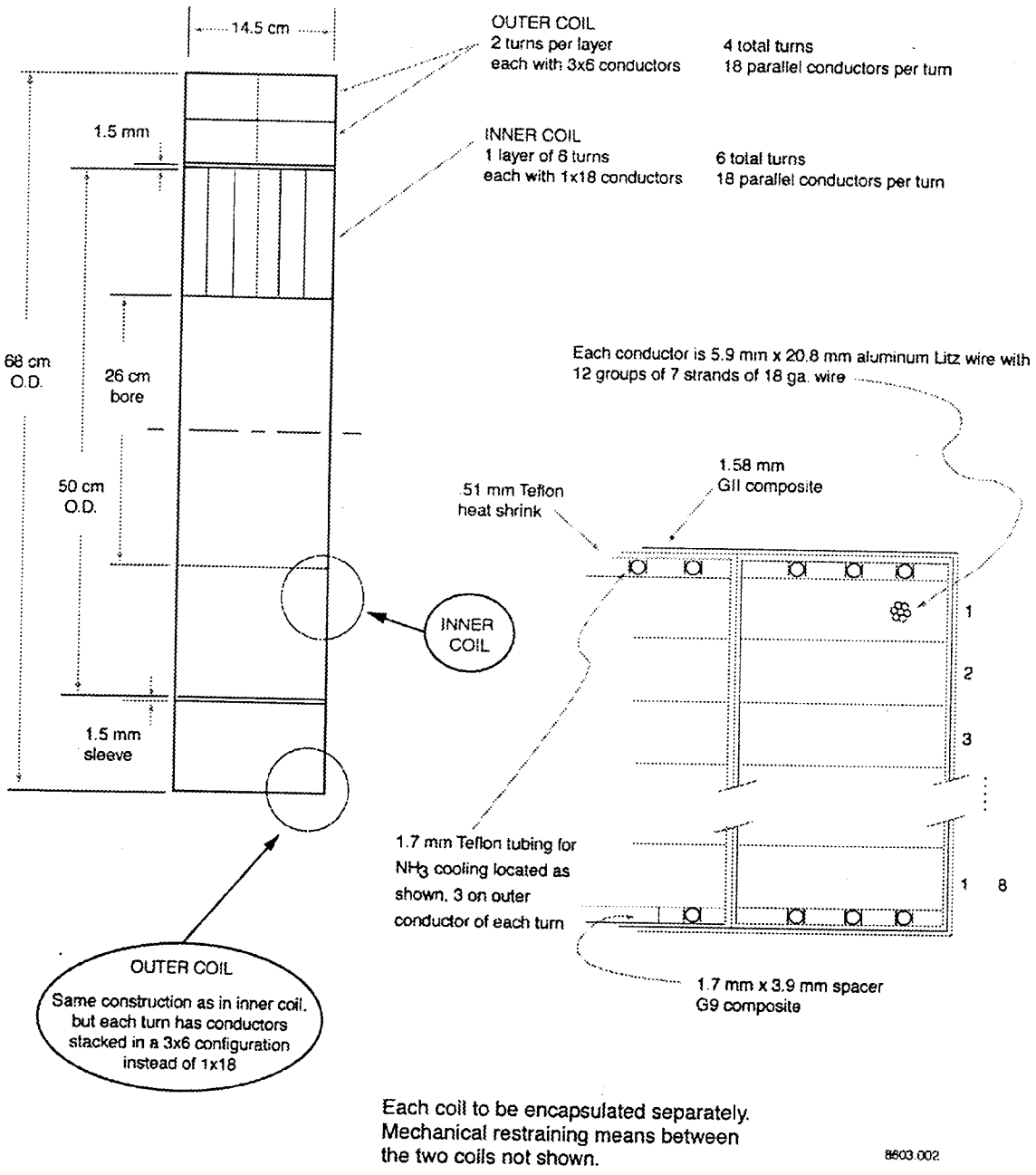

Figure 30. Autotransformer

REPORT DOCUMENTATION PAGE

Form Approved
OMB No. 0704-0188

1. AGENCY USE ONLY (*Leave blank*)	2. REPORT DATE	3. REPORT TYPE AND DATES COVERED
	June 2002	Final Contractor Report

4. TITLE AND SUBTITLE

SSP Technology Investigation of a High-Voltage DC-DC Converter

5. FUNDING NUMBERS

WU–732–4E–00–00
NAS3–00135

6. AUTHOR(S)

J.A. Pappas and W.M. Grady

7. PERFORMING ORGANIZATION NAME(S) AND ADDRESS(ES)

University of Texas at Austin
Center for Electromechanics
Austin, Texas 78712

8. PERFORMING ORGANIZATION REPORT NUMBER

E–13342

9. SPONSORING/MONITORING AGENCY NAME(S) AND ADDRESS(ES)

National Aeronautics and Space Administration
Washington, DC 20546–0001

10. SPONSORING/MONITORING AGENCY REPORT NUMBER

NASA CR—2002-211562

11. SUPPLEMENTARY NOTES

Contents were reproduced from the best available copy as provided by the authors. Project Manager, Patrick J. George, Power and Propulsion Office, NASA Glenn Research Center, organization code 6910, 216–433–2353.

12a. DISTRIBUTION/AVAILABILITY STATEMENT

Unclassified - Unlimited
Subject Category: 20 Distribution: Nonstandard

Available electronically at http://gltrs.grc.nasa.gov/GLTRS

This publication is available from the NASA Center for AeroSpace Information, 301–621–0390.

12b. DISTRIBUTION CODE

13. ABSTRACT ***(Maximum 200 words)***

The goal of this project was to establish the feasibility of a high-voltage DC-DC converter based on a rod-array triggered vacuum switch (RATVS) for the Space Solar Power system. The RATVS has many advantages over silicon and silicon-carbide devices. The RATVS is attractive for this application because it is a high-voltage device that has already been demonstrated at currents in excess of the requirement for an SSP device and at much higher per-device voltages than existing or near-term solid state switching devices. The RATVS packs a much higher specific power rating than any solid-state device and it is likely to be more tolerant of its surroundings in space. In addition, pursuit of an RATVS-based system would provide NASA with a nearer-term and less expensive power converter option for the SSP.

14. SUBJECT TERMS

Space solar power

15. NUMBER OF PAGES

54

16. PRICE CODE

17. SECURITY CLASSIFICATION OF REPORT	18. SECURITY CLASSIFICATION OF THIS PAGE	19. SECURITY CLASSIFICATION OF ABSTRACT	20. LIMITATION OF ABSTRACT
Unclassified	Unclassified	Unclassified	